Anisotropy of magnetic susceptibility impressed during rock magnetic procedures (AF, IRM) and information on the domain state of the magnetic carriers

Pierrick Roperch, Catherine Kissel, France Lagroix, Guillaume Dupont-Nivet, Annick Chauvin, Fernando Poblete, Jovid Aminov

▶ **To cite this version:**

Pierrick Roperch, Catherine Kissel, France Lagroix, Guillaume Dupont-Nivet, Annick Chauvin, et al.. Anisotropy of magnetic susceptibility impressed during rock magnetic procedures (AF, IRM) and information on the domain state of the magnetic carriers. Physics of the Earth and Planetary Interiors, 2023, 342, pp.107076. 10.1016/j.pepi.2023.107076 . insu-04170453

HAL Id: insu-04170453
https://insu.hal.science/insu-04170453

Submitted on 25 Jul 2023

HAL is a multi-disciplinary open access archive for the deposit and dissemination of scientific research documents, whether they are published or not. The documents may come from teaching and research institutions in France or abroad, or from public or private research centers.

L'archive ouverte pluridisciplinaire **HAL**, est destinée au dépôt et à la diffusion de documents scientifiques de niveau recherche, publiés ou non, émanant des établissements d'enseignement et de recherche français ou étrangers, des laboratoires publics ou privés.

Anisotropy of magnetic susceptibility impressed during rock magnetic procedures (AF, IRM) and information on the domain state of the magnetic carriers

Pierrick Roperch[a], Catherine Kissel[b], France Lagroix[c], Guillaume Dupont-Nivet[a], Annick Chauvin[a], Fernando Poblete[d], and Jovid Aminov[e,f]

[a] Géosciences Rennes, CNRS, Université de Rennes, Rennes, France, pierrick.roperch@univ-rennes1.fr

[b] Laboratoire des Sciences du Climat et de l'Environnement, CEA/CNRS/UVSQ, Université Paris-Saclay, CEA-Orme des Merisiers, Bat 714, Gif-sur-Yvette, France

[c] Institut de Physique du Globe de Paris, Université Paris Cité, CNRS, 1 rue Jussieu, 75005 Paris, France

[d] Departamento de Geología, Facultad de Ciencias Físicas y Matemáticas, Universidad de Chile, Chile

[e] Department of Earth and Environmental Sciences, University of Central Asia, 736000, Khorog, Tajikistan

[f] Institute of Geology, Earthquake Engineering and Seismology, National Academy of Sciences of Tajikistan, Dushanbe, 734063, Tajikistan

Abstract

We present and interpret anisotropy of magnetic susceptibility (AMS) fabrics in various rocks, focusing on the effects of Alternating Field (AF) demagnetization and Isothermal Remanent Magnetization (IRM). Our findings reveal that AMS in samples from intrusive rocks with large multidomain magnetite grains is minimally affected by IRM or static AF demagnetization. In nearly isotropic volcanic rocks with titanomagnetite pseudo single domain (PSD) carriers, AMS fabrics caused by static AF demagnetization are easily identifiable, with the most prominent effect being a well-defined AMS lineation (up to 1.04) in the direction of the applied AF demagnetization. Conversely, in samples from rapidly cooled volcanic rocks with titanomagnetite of smaller magnetic grain size, an AMS foliation (~1.02) is observed orthogonal to the direction of the applied AF field, instead of a lineation. In such samples, an IRM produces a much larger AMS foliation up to 1.3 orthogonal to the IRM. The IRM-impressed AMS is also particularly strong in metamorphic rocks in the greenschist facies with either titano-hematite or pyrrhotite magnetic carriers. Samples with the largest IRM-impressed fabric have very high M_{rs}/M_s ratio (> ~0.4). M_{rs}/M_s ratios above 0.5 may indicate the contribution of SD magnetic grains with multiaxial anisotropy. As the apparent multiaxial anisotropy is especially observed in volcanic rocks with micron size dendrites of titanomagnetites, the complex shape of the magnetic particles and their chemical composition likely play a key role in IRM-impressed AMS. AMS fabric in volcanic rocks should not be measured after static AF demagnetization. Tumbling AF demagnetization does not alter significantly the initial magnetic fabric and could be safely used in rocks with strong magnetization related to lightning possibly recording an IRM impressed AMS.

Keywords

AMS, Anisotropy of Magnetic Susceptibility, AF demagnetization, Isothermal Remanent Magnetization

1. Introduction

Anisotropy of the magnetic susceptibility (AMS) measurements are a standard and convenient tool to infer fabrics due to rock formation and deformation processes (Borradaile and Henry, 1997; Hrouda, 1982; Rochette et al., 1992). However, the relationship between the AMS orientations and the rock's fabric may be altered by other laboratory protocols commonly used in paleomagnetic studies. Field-impressed Anisotropy of Magnetic Susceptibility (AMS) in samples exposed to large direct fields (DF) or alternating fields (AF) has long been recognized in samples with single domain (SD) and multidomain (MD) magnetite particles (Bhathal and Stacey, 1969; Potter and Stephenson, 1990a, 1990b; Violat and Daly, 1971). More recent studies have mainly discussed the effect of AF on AMS (Biedermann et al., 2017; Henry et al., 2007; Jordanova et al., 2007; Liu et al., 2005; Schöbel et al., 2013). *Biederman et al.* (2017) studied the effect of static AF demagnetization upon 4 sets of samples from different rock types. AF demagnetization had only marginal effects on slates, red beds and intrusive rocks with initial strong magnetic fabrics (i.e. high degree of anisotropy). However, for basaltic rocks with low initial anisotropy, they observed impressed prolate ellipsoids with lineations coaxial to the direction of the applied AF field and degree of anisotropy as high as 1.02.

The observation of a highly pervasive AF impressed AMS in a large collection of Holocene volcanic rock samples from volcanic zone of south-central Chile motivated us to follow up

on the study by Biederman et al. (2017). The second motivation for the study of strong field impressed AMS came from the observation of a significant control of the AMS by Isothermal Remanent Magnetization (IRM) in sedimentary rocks affected by greenschist metamorphism and titanohematite as the main magnetic carrier (Aminov et al. submitted).

While AF impressed AMS has long been documented, Rochette et al., (1992) indicated that the effect of an imparted IRM on the AMS had not clearly been addressed. This was the subject of a few early on studies (Potter and Stephenson, 1990a) recently followed by a few more studies (e.g. Lanci, 2010). The application of an IRM was suggested to have a stronger effect than an AF field (Potter and Stephenson, 1990; Lanci, 2010) but the relative effect of AF or IRM on AMS and their potential cause remain largely unconstrained despite the biases that these effects may introduce on data interpretation. Moreover, whether and how an AF or IRM modifies an initial AMS may have a diagnostic (mineral or domain state) potential or lead to the development of new experimental procedures. We thus carried out an extensive study of the effect of IRM on AMS in order to compare AF and IRM impressed AMS. On a variety of rock types, we show how the AMS changes upon application of AF or a direct field (DF). Following previous work on an IRM impressed magnetic foliation in glassy parts from pillow lavas (Lanci, 2010), our study extends the investigation to a wider range of lithologies from red beds, metamorphic sediments, and volcanic and intrusive rocks with various magnetic mineralogies. Overall, the collected data and observations allow us to better characterize IRM impressed AMS in different rock types and we propose potential acquisition mechanisms related to specific rock magnetic properties.

2. Methods and Materials

2.1 Methods

An AMS ellipsoid is characterized by the magnitude and orientation of the three principal axes with $K_1>K_2>K_3$. The degree of anisotropy is K_1/K_3 while the foliation is K_3/K_2 and the lineation is K_1/K_2. Several parameters are often used to describe the shape and eccentricity of the AMS ellipsoid (see also Bilardello and Biedermann, 2022). In this article we will used the shape parameter T and eccentricity parameter P' defined by Jelinek (1981) as:

$P' = \exp \sqrt{2[2(n_1 - n)^2 + (n_2 - n)^2 + (n_3-n)^2]}$

$T = (2n_2 - n_1 - n_3)/ (n_1-n_3)$; where n_1, n_2, n_3 are respectively the natural logarithms of the principal susceptibilities k_1, k_2 , k_3 and $n =(n_1+n_2+n_3)/3$

AMS fabrics were measured with the AGICO KLY3-S kappabridge prior and after IRM acquisition and/or static AF demagnetization with 2G online AF degausser or the Schonsted degausser (Géosciences Rennes laboratory). The AMS of a few samples were measured with the AGICO MFK1 (at the CEREGE laboratory) instrument using the low and high frequency and the AGICO MFK2-FA (LSCE) was used to check the field dependence of the AC susceptibility in the field range of 5 – 700 Am^{-1}. The KLY3 used an effective field of 300 Am^{-1} equivalent to a peak field of ~425 Am^{-1} while the MFK1 and MFK2 use a peak field of 200 Am^{-1} in the standard procedure. The out-of-phase signal was measured with the KLY5 at the Géosciences laboratory in Toulouse.

IRMs were acquired with an ASC pulse magnetizer usually up to 1 T except for samples with hematite for which we used 2.3 T, the largest possible field for cylindrical standard size samples (25 mm in diameter and 22 mm height). The remanent magnetization was measured with the JR6 AGICO spinner magnetometer. Hysteresis cycles were obtained with the AGM-2900 or the VSM-8600 at the LSCE laboratory. Thermal demagnetizations of IRM were performed with a MMTD furnace. A few samples demagnetized by static field or having a SIRM were later demagnetized at 100 mT with the AGICO LDA5 AF demagnetizer (at the CEREGE laboratory) using a tumbler and a linear and fast AF decrease rate. Scanning electron microscope images were obtained with a JEOL JSM 7100 F coupled with an EDS EBSD Oxford for element composition.

The impressed fabric T_i was determined by subtracting the normalized original fabric T_0 from the normalized fabric measured after AF or IRM application T_1. $T_i = (T_1 – T_0 + I)$, where I is the identity matrix. With this approach, we do not consider that the enhancement or decrease in magnetic susceptibility after application of an IRM or AF affects the fabric (see discussion below). We attribute the mean susceptibility related to T_1 to the mean susceptibility associated to the difference ellipsoid T_i.

The AMS fabric impressed by IRM (AMS_{IRM}) or AF (AMS_{AF}) is the difference between the two AMS tensors prior and after IRM acquisition or AF demagnetization, both normalized by their respective Kmean values. By subtracting the after from the before AMS, whatever remains unchanged, will be de facto excluded. This is obviously the case for the contribution to the AMS of the paramagnetic carriers. If the sample is isotropic prior to the application of an AF or IRM, the calculated tensor difference equals that of the second tensor.

2.2 Sample selection

In this study, we investigated more than 300 specimens stemming from 4 main suites of samples and other miscellaneous specimens (supplementary Table S1).

A first suite of 57 specimens of late Cretaceous volcanoclastic sediments from the Central Pamir (Aminov et al. submitted) was investigated. These rocks are deformed and record a greenschist metamorphism with fine-grained biotites dated to the Early Miocene by $^{40}Ar/^{39}Ar$. The main oxide is a 10-100 µm titanohematite with inclusions of rutile and the presence of nanometer thin rutile lamella does not permit any accurate chemical analysis due to the spatial resolution of EDS-SEM analyses (**Supplementary Figure S1**). We did not identify ilmenite lamella in the oxide grains. Their bulk magnetic susceptibilities range from $1 – 3\ 10^{-4}$ SI. Saturation during IRM acquisition is observed in between 0.3 and 1 T (**Supplementary Figure S2**).

The unblocking temperature of saturation IRM is about 620 °C in agreement with the systematic presence of 5 to 10 % of titanium detected by EDS analyses within the titanohematite. We did not observe the Morin transition in low temperature experiments supporting the interpretation that the main oxide mineral is titanohematite and not hematite (**Supplementary Figure S3**).

A second suite of 154 specimens from Chilean Holocene volcanics were drilled in rapidly-cooled basaltic juvenile clasts in pyroclastic density currents (Roperch et al., 2014) and in

massive lava flows and lava flow-tops (Roperch et al., 2015). Titanomagnetite is the main magnetic carrier in these rocks with a wide range of Curie temperatures (supplementary Fig. S4). In samples from lava flow tops, remanence saturation is found below 250 mT at room temperature. There is no evidence of the Vervey transition for magnetite but there is a higher coercivity phase observed at 20 K supplementary Fig. S3). In the basaltic juvenile clasts, it is difficult to image iron oxides, even with a SEM due to the small size of the magnetic grains. In the rapidly cooled parts of the lavas, titanomagnetite is mainly observed as dendrites (supplementary Fig. S1) instead of 1 to 10 μm titanomagnetites grains observed in samples from the interior of the lava flows.

Cenozoic volcanic specimens (n = 35) from Southern Peru were also investigated and correspond to lava flows with titanomagnetite to ignimbrite with variously oxidized magnetic minerals.

A fourth suite of specimen groups together Cenezoic redbeds of sandstones and siltstones from Tadjikistan (Li et al., 2022) (n = 31) with detrital hematite as the main magnetic carrier and from Tibet (n = 10) with hematite and chemical remagnetization (samples listed in supplementary Table S1).

Other specimens investigated in this study are magnetite-bearing intrusive granodiorites from Miocene stocks in Central Chile and Cretaceous batholith in the Andes, pyrrhotite-bearing metamorphic sediments from Patagonia (Poblete et al., 2016), and titanomagnetite-bearing historical bricks from Central Chile (Roperch et al., 2015).

3. Magnetic susceptibility changes

Following the application of an IRM or after an AF demagnetization, we observe variable change in bulk volume specific mean magnetic susceptibility (κ) (Fig. 1) compared to the initial state.

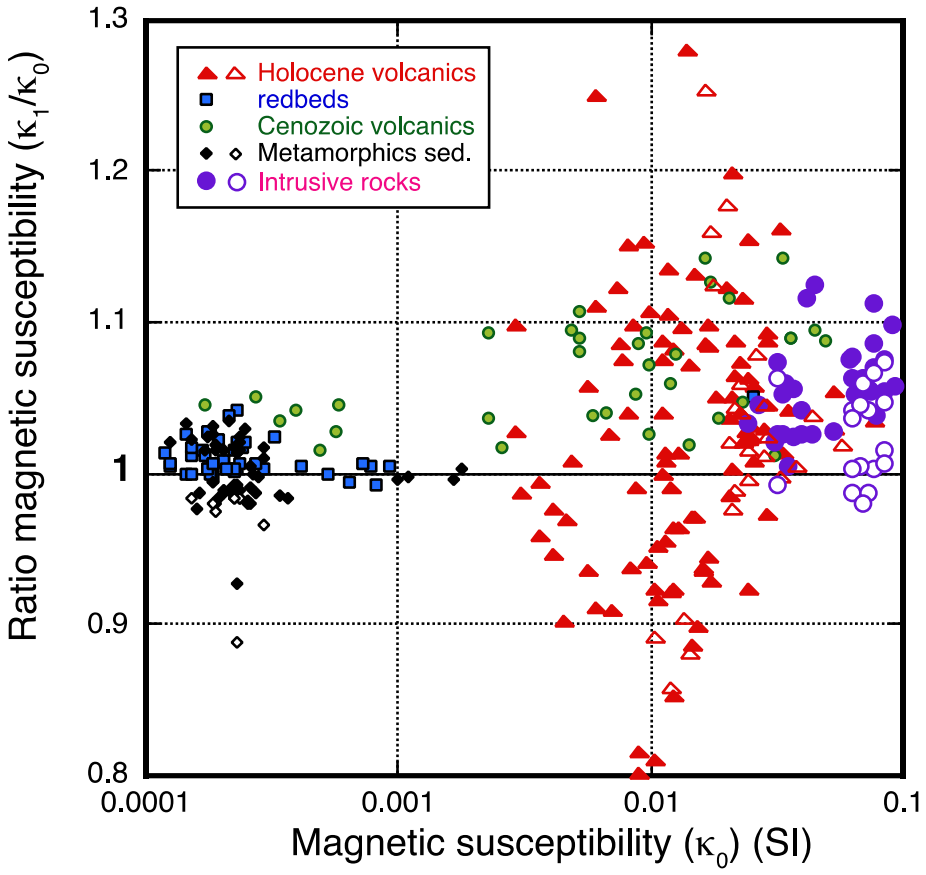

Fig. 1. Ratio κ_0/κ_1 of the magnetic susceptibility (KLY3 instrument) after application of an IRM (filled symbols) or after AF demagnetization (open symbols) (κ_1) to the susceptibility at the initial state (κ_0) versus κ_0.

Samples with low κ and mainly hematite or titano-hematite as the magnetic carrier do not show significant variation in κ after application of an AF or IRM unlike most of the other samples. The largest range of κ_1/κ_0, from 0.8 to 1.3, is observed for Holocene lava flows with titanomagnetite as the main magnetic carrier. The κ of these Holocene volcanics is sensitive to changes in temperature with a significant increase from room temperature to about 150°C (**Supplementary Figure S4**). However, even if the temperature of the room where the measurements were made changed by a few degrees during the experiments, it cannot account for the observed very large changes in κ as reported in Fig. 1.

Upon application of an AF, we observe in most samples that the change in magnetic susceptibility occurs at intermediate fields (~<30-50 mT) and further field increase do not significantly change the susceptibility. An example is given for one sample from a lava flow with an increase of 1.28 in magnetic susceptibility after the AF demagnetization at 70 mT along X. Applying the AF along Y and Z at 70 mT does not further change the magnetic susceptibility. The same observation is made after further application of an IRM at 75 mT and 250 mT (**Supplementary Figure S5**).

The major changes in magnetic susceptibility after AF demagnetization are observed in samples with κ strongly dependent on the AC field used for the susceptibility measurement (Fig. 2 and **Supplementary Figure S5**). An increase by up to a factor 2 is observed within the range of fields available with the MFK2 consistent with previous observations (Jackson et al., 1998). Samples from plutonic rocks with magnetite as the main magnetic carrier do not show such susceptibility dependence on AC fields (supplementary Table S1).

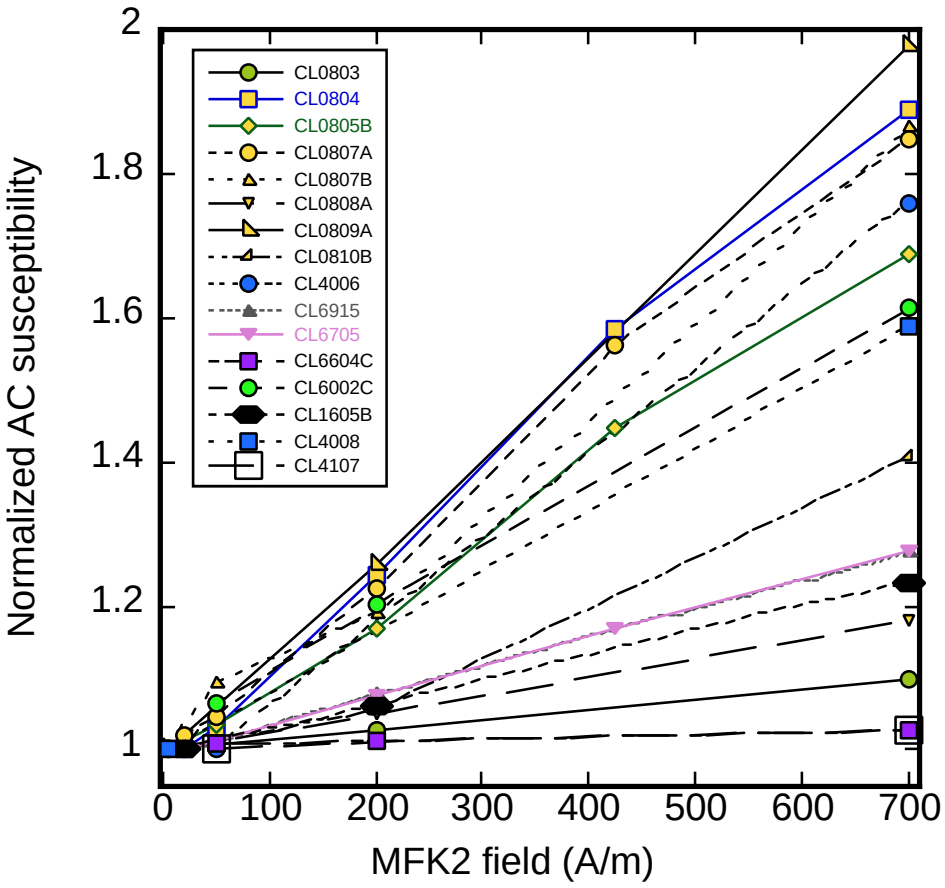

Fig. 2. Variation of the magnetic susceptibility versus the peak magnetic field available with the MFK2 instrument. Values are normalized to the one acquired at the lowest used field <= 50 A/m. Samples are from the set of Holocene volcanic rocks.

4. Alternating field impressed AMS (AMS$_{AF}$)

In a routine analysis of AMS on samples from the Holocene volcanic zone of south-central Chile, some AMS measurements were done on samples previously demagnetized by static AF. There, AMS measured after a sequence of alternating (YZX or XZY) static AF demagnetizations resulted in a well-defined prolate ellipsoid with its maximum axis parallel to the direction of the last applied field (X or Y, respectively) (Fig. 3) as described by Biederman et al. (2017). But samples from sites sampled in the rapidly cooled upper surface of a lava flow departed from this behavior with an oblate fabric characterized by a minimum axis coaxial to the direction of the last applied AF field.

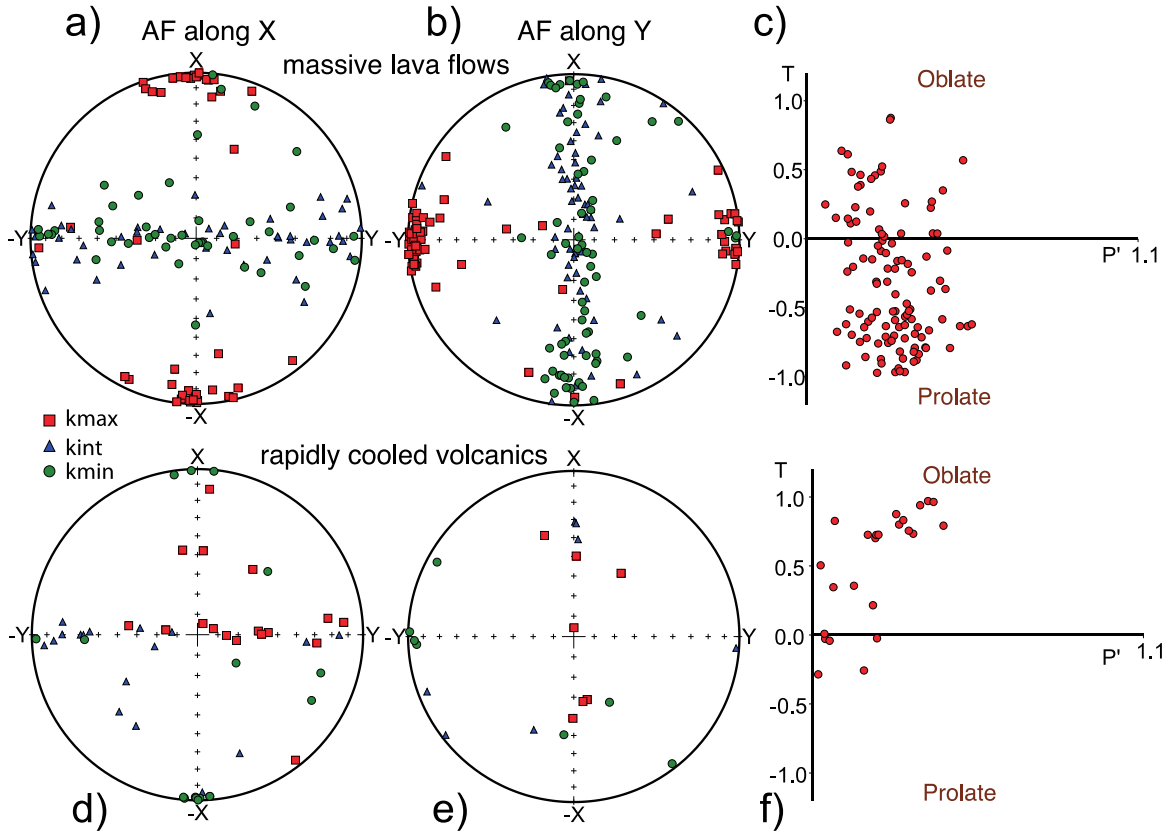

Fig. 3. AMS data in samples from Holocene lavas processed by static AF demagnetization. a, b, c: samples in the massive parts of lava flows; d, e, f: samples in rapidly cooled lavas flow top and juvenile clasts. a, b, d, e: Equal-area plot of the AMS directions for samples demagnetized with the last step, usually in between 80 to 120 mT with the sequence YZX (a, d) and XZY for (b, e); c, f) T-P' plot of the shape of the ellipsoid (T) versus corrected anisotropy degree (P') (Jelinek, 1981). Data in supplementary Table S1.

As discussed previously, the application of a static AF demagnetization induces a change in bulk magnetic susceptibility (Biedermann et al., 2017; Jordanova et al., 2007). Although no further change in mean susceptibility is observed in successive applications of an AF above 30 mT, a change is observed in AMS: an AMS lineation created by an AF field along X, re-aligns with the last direction along which the AF is successively applied (Y or Z) (Fig. 4). While it is not possible to return to the initial magnetic susceptibility, the process of AMS_{AF} can be repeated. For this reason, as explained above, the difference of AMS ellipsoids is calculated on κ_{mean} normalized tensors. This makes easier the comparison of the results between samples, in particular because the degree of anisotropy of the AF impressed anisotropy is directly comparable to that of the AMS usually found in rocks.

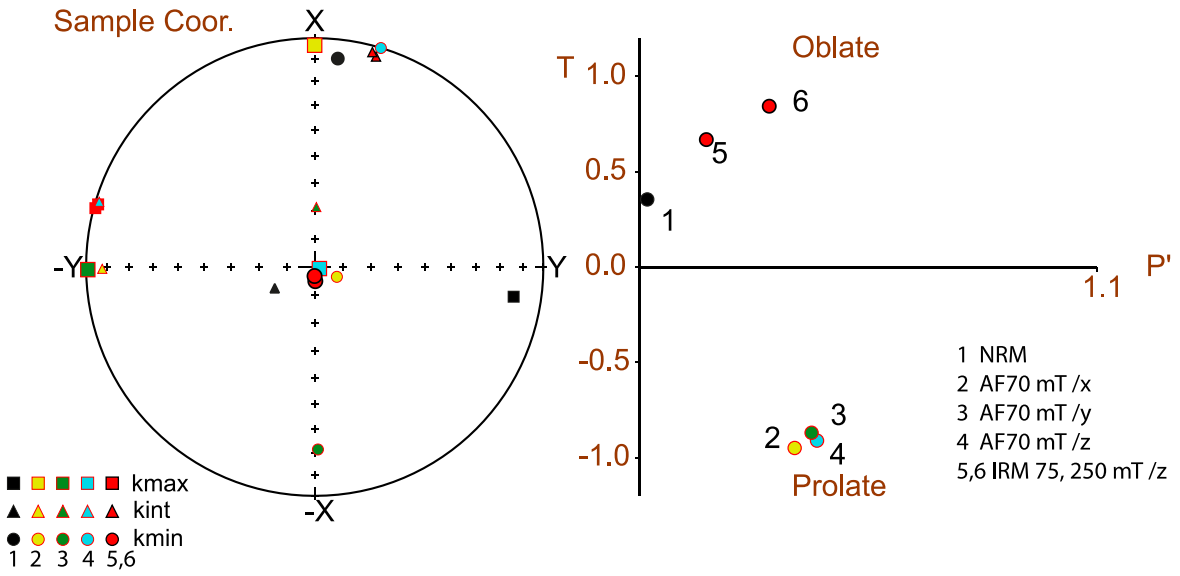

Fig. 4. Changes in AMS orientation upon application of a static AF field at 70 mT along X, Y and Z and by a DF field at 75 and 250 mT along Z. N0 is the initial AMS state. Left: Equal-area plot of the main directions of AMS ellipsoids; right: Changes in the shape of anisotropy T versus the corrected anisotropy degree P' (Jelinek, 1981). Sample CL0805B from Holocene volcanic rocks.

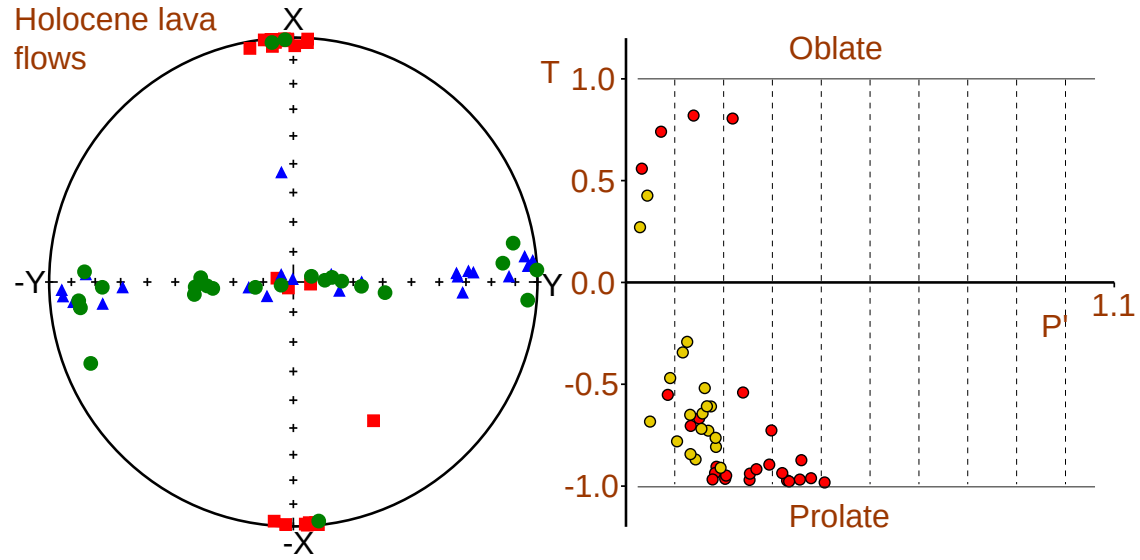

Fig. 5. Impressed anisotropy (difference ellipsoids) by static AF demagnetization at 70 mT along X for Holocene lavas. Left: Equal-area plot of the main directions of AMS ellipsoids; right: Changes in the shape of anisotropy T versus the corrected anisotropy degree P' (Jelinek, 1981). Red dots: this study; results for the Fogo samples (Biederman et al., 2017) (yellow dots) are shown for comparaison on the T-P' plot.

Biederman et al. (2017) found that the impressed anisotropy during AF demagnetization was almost not changing above 30 mT for the group of basaltic samples. We also found the same evidence and this is why we choose a slightly higher value of 70 mT for the experiments and not the highest field value available for the degausser. A well-defined prolate fabric elongated along X which is the direction of the AF field applied along X is observed in all samples but four which show a trend toward an oblate AMS_{AF} (Fig. 5). We will see later that samples with an AMS_{AF} oblate fabric have also a strong AMS_{IRM} oblate fabric. In addition to the AF impressed prolate fabric, some samples show strong AC field dependence on κ_{mean} and on the magnitude of the lineation (Fig. 6). However, a strong AC field dependence on κ_{mean} is not observed for all samples showing a well-defined AF impressed lineation. For example, specimen CL0803a from the same lava flow as those samples shown in Fig. 6 records a strong AF impressed AMS lineations of 1.029 measured with the KLY3 but a limited increase in κ by only 9% from 5 to 700 A/m (supplementary Table S1).

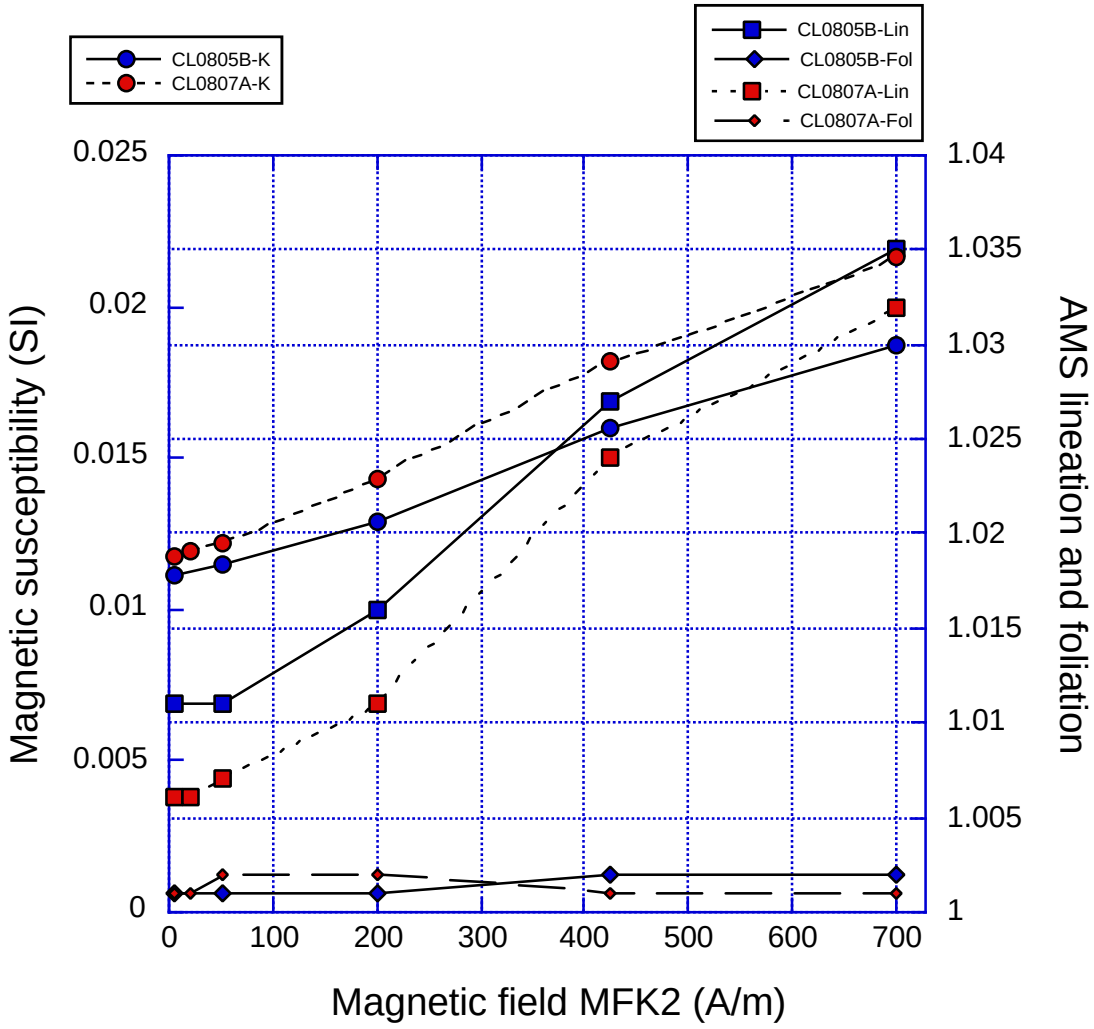

Fig. 6. Examples of changes in mean magnetic susceptibility (circles), magnetic lineation (squares) and magnetic foliation (diamonds) as a function of MFK2 AC applied field for two samples of one Holocene volcanic flow (CL0807A in red; CL0805B in blue).

Consequently, the lower magnitude of the magnetic lineation obtained for the Fogo samples (Fig. 5) compared to that of Holocene lavas is possibly due to the difference in standard peak fields between the MFK1 (200 Am^{-1}) used in Biederman et al. (2017) for the Fogo samples and the KLY3 (425 Am^{-1}) used in the present study. It is thus critical to calculate the difference ellipsoids for AMS measured at the same AC applied field and frequency values.

The orientation of the AMS_{AF} ellipsoid is easily modified by successive applications of the high static AF fields and this AF impressed anisotropy is removed with a tumbler (supplementary Table S1).

An AF impressed lineation is also observed in intrusive rocks (**Supplementary Figure 6**). The magnetic lineation is slightly less well defined than in volcanic rocks without a significant initial AMS (supplementary Table S1). In intrusive rocks with an initial degree of anisotropy greater than 1.05, a field impressed anisotropy does not significantly change the initial anisotropy.

5. IRM impressed AMS (AMS_{IRM})

An IRM acquisition typically shifts the minimum axis of the susceptibility tensor along the direction of the applied field (Fig. 4). This effect is clearly seen in most of our Holocene volcanic samples where an AMS_{IRM} replaces an AMS_{AF}. Applying an AF field at 70mT following the IRM reverts the impressed fabric from oblate to prolate in samples with a low IRM impressed foliation (~1.03). Measuring an AMS_{IRM} can be performed with samples previously AF demagnetized. In this case, the initial fabric subtracted to determine the tensor difference should be either the initial state prior to static AF demagnetization or the one after AF tumbling but not the fabric measured after the static AF application.

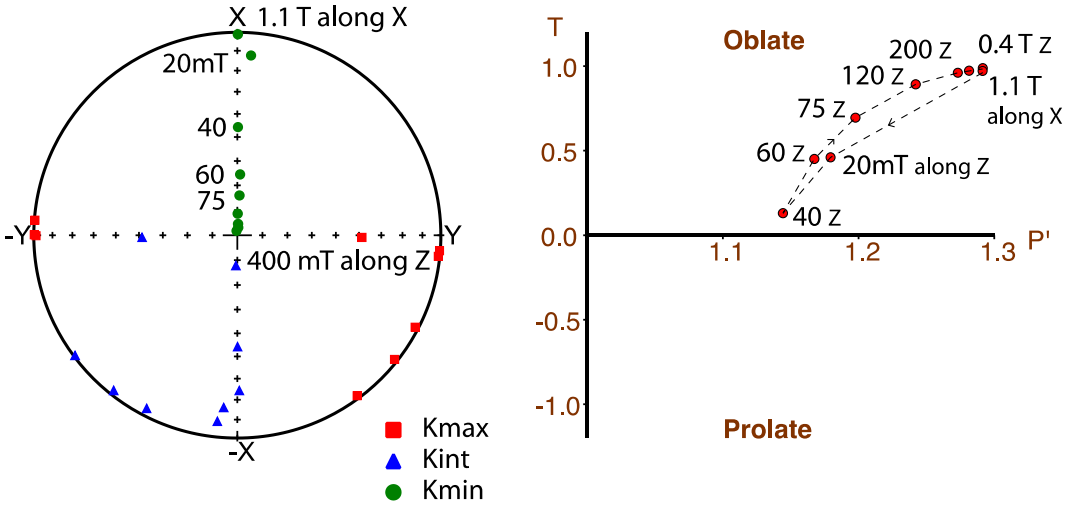

Fig. 7. Changes in AMS_{IRM} when an IRM is progressively acquired (20,40, 60, 75, 120, 200, 250, 400 mT) along the Z axis from an initial saturation (1.1T) given along X (sample CL4118, juvenile basaltic clast). Left: Equal-area plot of the main directions of AMS ellipsoids; right: Changes in the shape of anisotropy T versus the corrected anisotropy degree P' (Jelinek, 1981).

5.1 AMS behavior during progressive IRM acquisition.

Acquisition of AMS_{IRM} is only dependent on the direction and intensity of the IRM. In order to test the effect on an AMS_{IRM} of a saturation IRM by a following IRM in another direction, we measured the AMS after each step of a progressive IRM acquisition along the Z axis following a full acquisition (IRM saturation) along the X axis (Fig. 7). The foliation initially acquired orthogonal to the X axis was progressively removed resulting in a decrease of the degree of anisotropy and the formation of a tri-axial ellipsoid. For fields higher than 40 mT, the degree of anisotropy increases again with the final formation of a foliation orthogonal to Z. This observation and behavior of the AMS is reminiscent to what is expected when successive phases of deformation are added (Borradaile and Henry, 1997).

Examples of the relation between IRM acquisition, mean magnetic susceptibility and AMS is also shown in **Supplementary Figure S2** for the metamorphic volcanoclastic samples with titanohematite from the Pamir.

In the following sub-sections, we present the effects on AMS of an IRM acquired along the Z axis above saturation (or at 2.3 T for the red beds) for five sets of samples with different lithologies and different magnetic mineralogies.

5.2 Holocene volcanic rocks

A total of 95 samples from Holocene volcanic rocks from the southern volcanic zone of Chile were processed. Most of the samples are from rapidly cooled volcanic units and some are from the dense massive part of the lava flows. The initial AMS fabric is in most case isotropic especially in the rapidly cooled units. The application of an IRM in rapidly cooled volcanics greatly changes the magnetic fabric with an impressed magnetic foliation plane orthogonal to the direction of the IRM and a degree of foliation greater than 1.3 in some samples (Fig. 8). We can also highlight the efficiency of the difference ellipsoids in removing the initial fabric (Fig. 8) supporting the assumption that the initial AMS is not carried by the oxides recording the AMS_{IRM}.

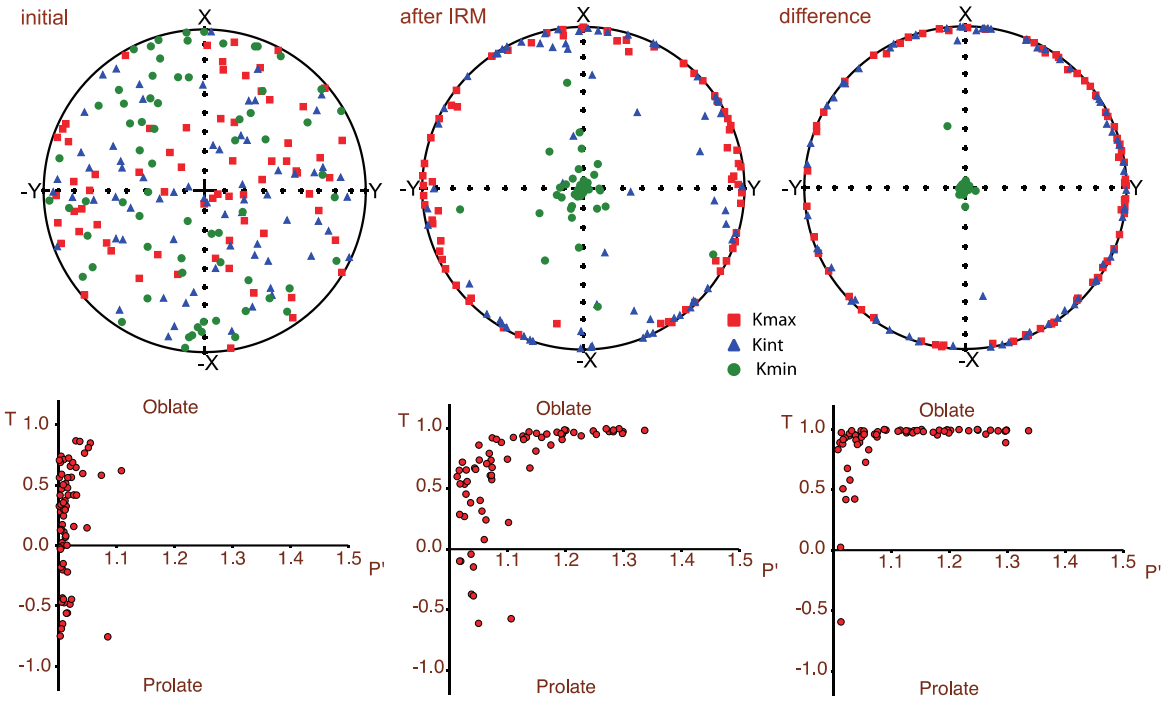

Fig. 8. AMS data for Holocene volcanics from central Chile, before and after IRM acquisition and the calculated tensor difference. Top: Equal-area plot of the main directions of AMS ellipsoids; bottom: Changes in the shape of anisotropy T versus the corrected anisotropy degree P' (Jelinek, 1981).

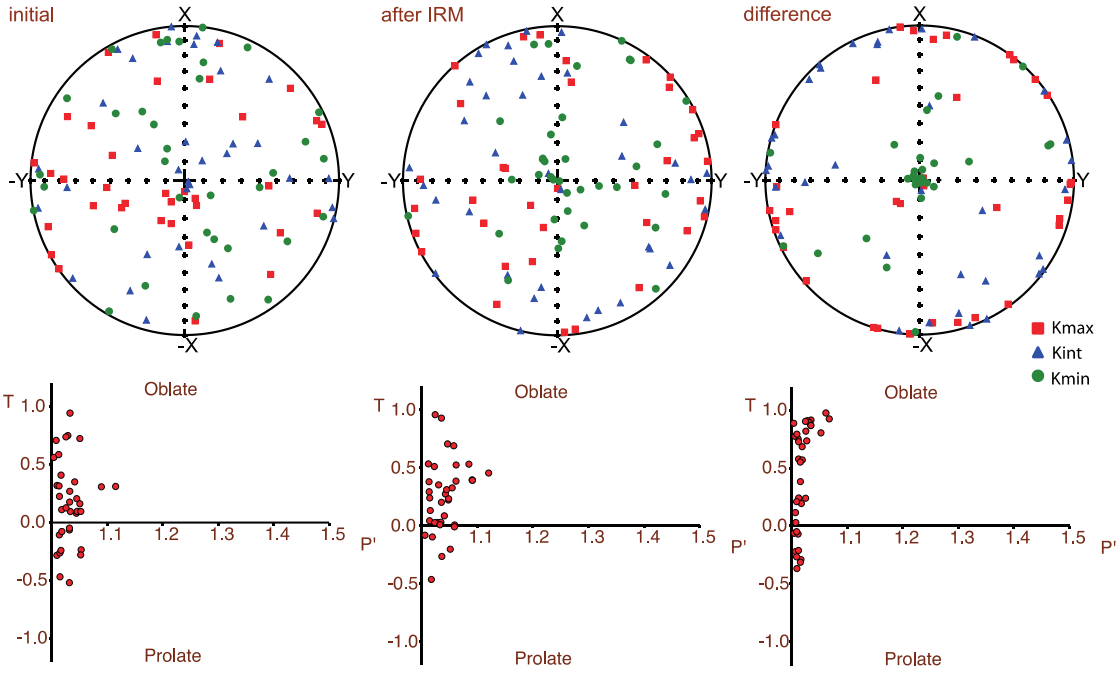

Fig. 9. AMS data for Cenozoic volcanics from Peru, before, after IRM acquisition and the calculated tensor difference. (legend as in Fig. 8).

5.3 Cenozoic volcanics from Peru

The rapidly cooled flow tops or juvenile clasts in pyroclastic deposits, that are well observed in Holocene or recent volcanic deposits, are fragile units, usually eroded in older volcanic rocks. Cenozoic volcanic samples from Southern Peru are thus more representative of volcanic rocks sampled in most paleomagnetic studies. An IRM impressed AMS fabric is also observed but its degree of anisotropy is much lower than in samples from rapidly cooled Holocene volcanic units and similar to the massive interior of recent lavas (Fig. 9).

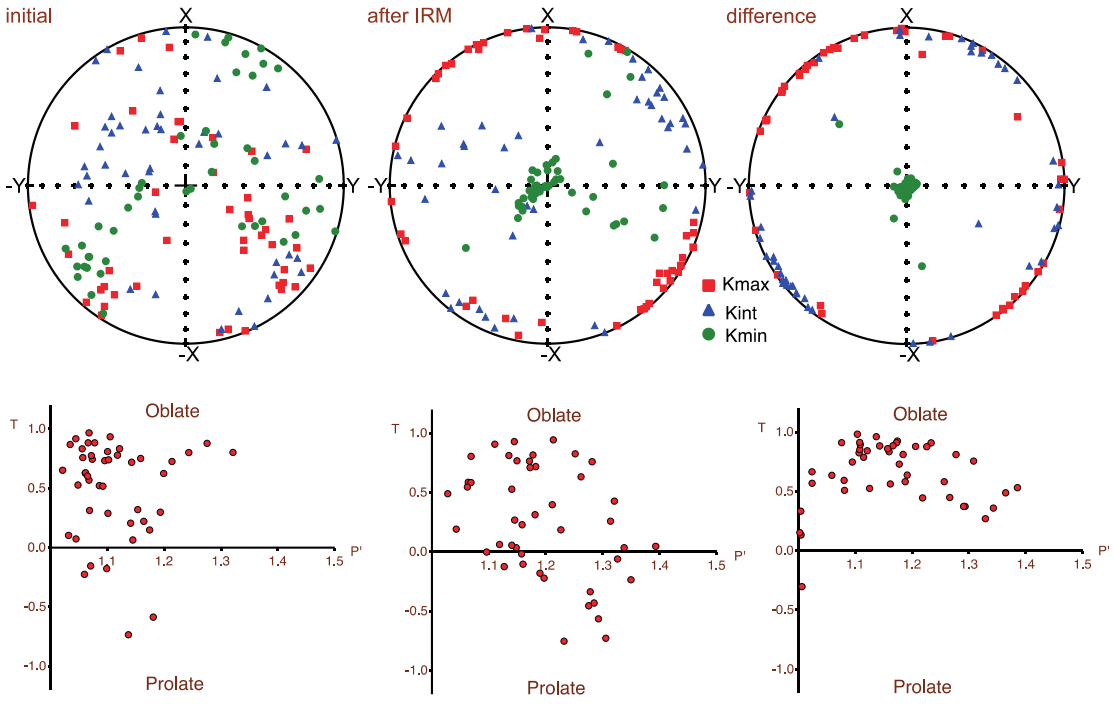

Fig. 10. AMS data for metamorphic volcaniclastic rocks with titanohematite before and after IRM acquisition and the calculated tensor difference. (legend as in Fig. 8).

5.4 Metamorphic volcanoclastic rocks with titanohematite (Pamir)

These samples have an initial AMS fabric due to compressive deformation associated with metamorphism (Aminov et al., submitted).

The experiments on AMS_{IRM} were performed on natural samples and samples previously heated in air up to 680°C. The decision to use demagnetized samples is based on two factors: first, the wide availability of samples that have already been demagnetized after a conventional paleomagnetic study, and second, to test the stability of the magnetic phase at high temperature. During IRM acquisition, the degree of AMS_{IRM} increases with increasing field of IRM acquisition, while the mean bulk magnetic susceptibility does not change (**Supplementary Figure S2**). For the previously heated sample set, a slight increase in coercivity of remanence is observed and the degrees of AMS_{IRM} are slightly lower values than for the unheated set of samples. Slight oxidation or some kind of annealing during laboratory heating

in air above 600°C may explain the slight difference between the two sets of samples. Mean magnetic susceptibility during IRM acquisition remains unchanged in both sets of samples.

In sample coordinates, the axes of the initial AMS fabric are randomly distributed (Fig. 10). Again here, the fabric is better organized after IRM acquisition, with a foliation plane nearly orthogonal to the Z axis. This impressed foliation is better defined after the removal of the initial fabric although not perfect as shown by the not fully oblate shape on the T-P' plot. This is likely due to an initial AMS fabric carried by paramagnetic minerals and iron oxides: while the paramagnetic contribution is removed in the tensor difference, the initial fabric of the oxide minerals is likely also partially reset by the IRM. This is likely the reason why the tensor difference is not fully oblate as the one found in the Holocene volcanics (Fig. 8) with an isotropic initial AMS fabric. A maximum degree of AMS_{IRM} of 1.8 was found in one sample of the Pamir metamorphic volcanoclastic rock with titano-hematite (not shown on Fig. 10).

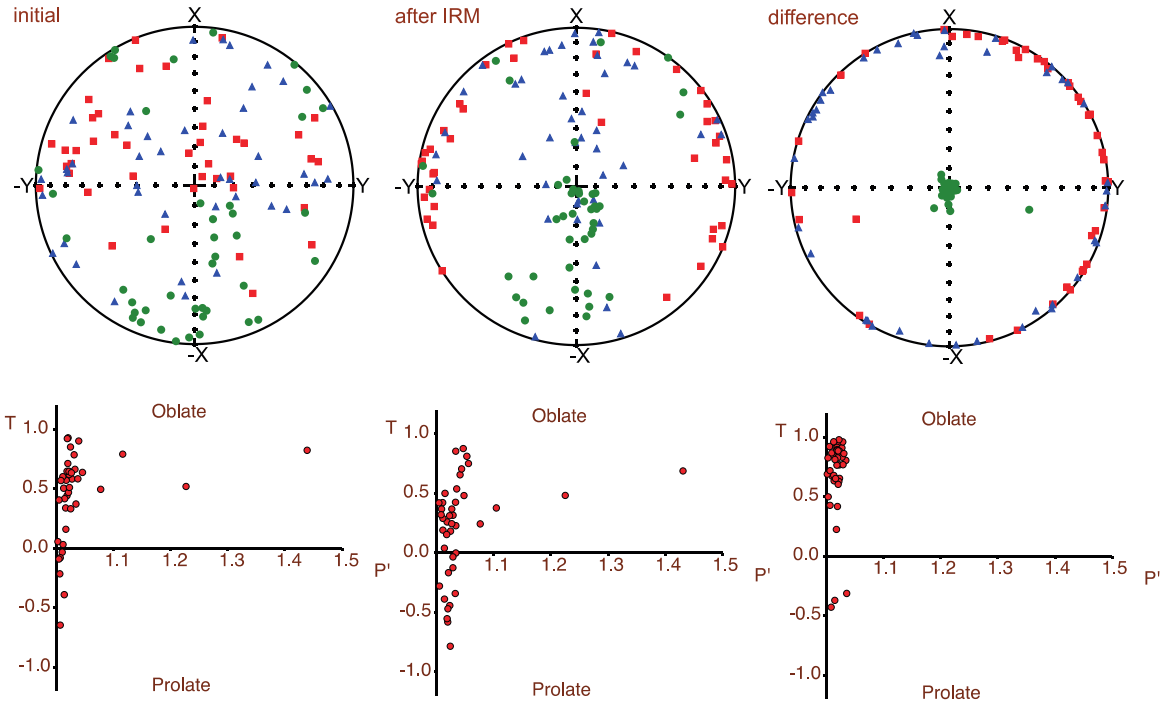

Fig. 11. AMS data for red beds, before, after IRM acquisition and the calculated tensor difference. (legend as in Fig. 8).

5.5 Red beds

Red beds present a low degree of AMS_{IRM} with a well-defined foliation after removal of the original fabric. This foliation is especially well observed in the samples from the Tajikistan Miocene sandstones (Li et al., 2022) with an IRM impressed foliation of 1.018 (Fig. 11). Although further work is needed, samples from red beds with chemical magnetizations seem to be less prone to an impressed AMS fabric than samples with detrital hematite.

5.6 Intrusive rocks

AMS fabrics in samples from intrusive rocks are the least sensitive to IRM. The orientations of the ellipsoid principal axes are not significantly changed after IRM acquisition and the fabric of tensor difference has a low degree of anisotropy without any clear preferentially orientation of the fabric, contrasting significantly with all other types of rock (Fig. 12).

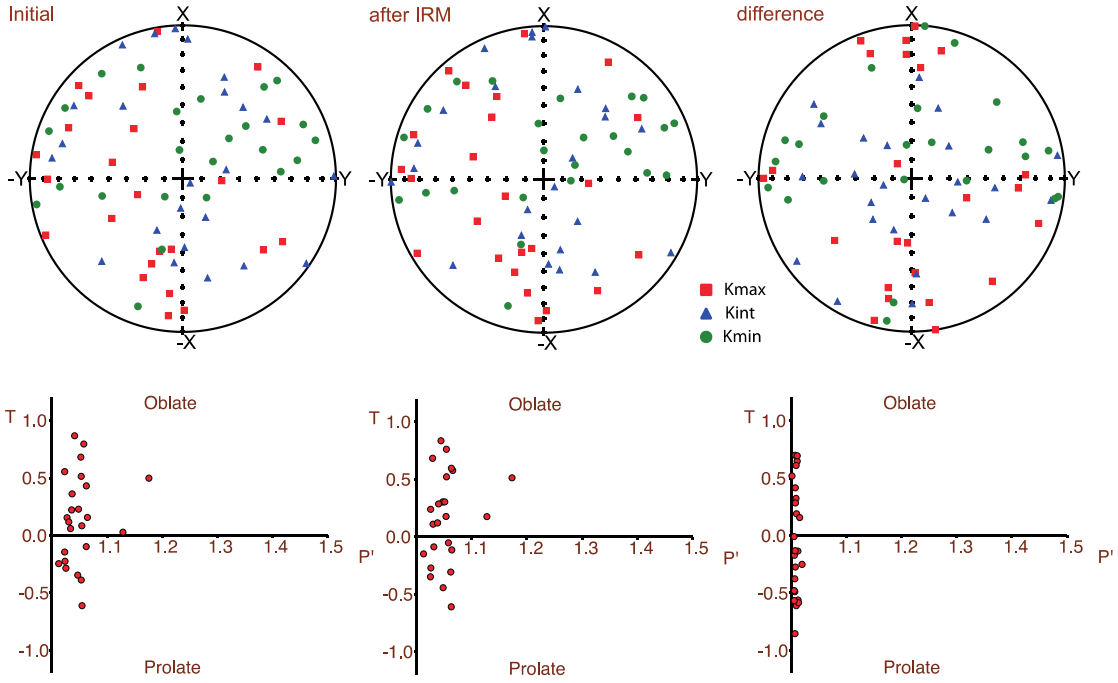

Fig. 12. AMS ellipsoids for intrusive rocks, before and after IRM acquisition and the calculated tensor difference. (legend as in Fig. 8).

6 Rock magnetic properties and AMS_{IRM}

Samples with large AMS_{IRM} foliations (up to ~1.3) also present a slight foliation after static AF demagnetization while those with a well-defined lineation after AF demagnetization show a much reduced AMS_{IRM} foliation (< ~1.03).

For volcanic rocks, the AMS_{IRM} foliation is especially well developed in samples with high ratios of saturation IRM versus low field bulk susceptibility. Despite the very different lithologies and nature of the magnetic carriers, sediments and metamorphic rocks show the same relationship (Fig. 13a). Samples with the largest AMS_{IRM} foliation correspond to those with the largest ratio of IRM/κ. Therefore, high ratios of IRM/κ seem to be a first order indicator for an easy acquisition of a IRM impressed AMS.

6.1 Hysteresis parameters

As seen in the description of AMS_{IRM} in the five typical rock types, the lithology of the samples is important to take into account as well as the iron oxide grain size. This is

confirmed by the hysteresis parameters as reported on a Day plot (Fig. 13b, **Supplementary Figure S7**).

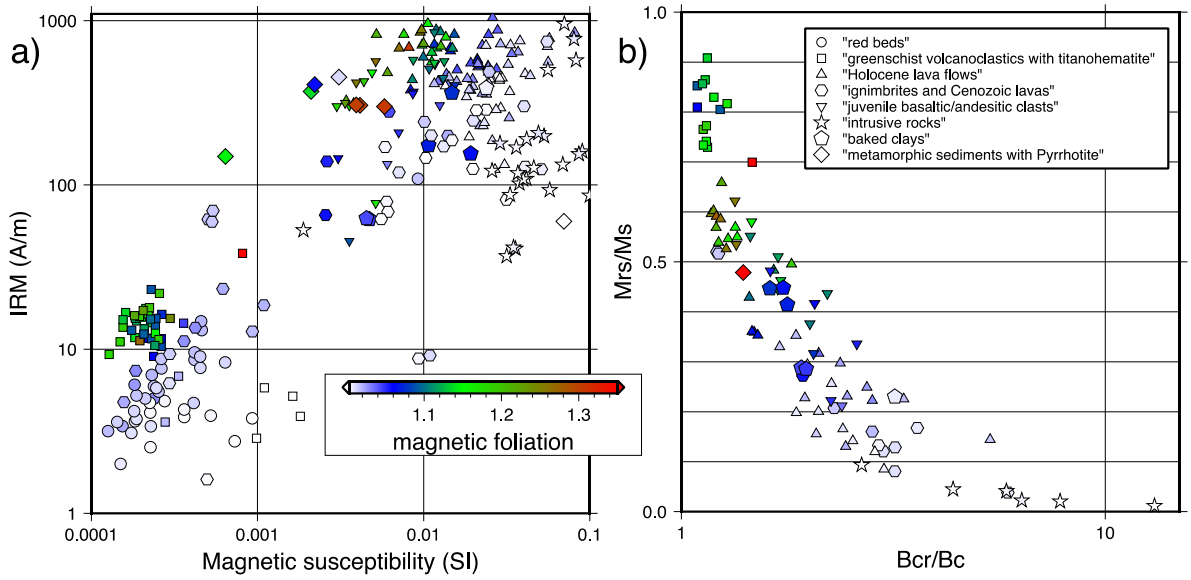

Fig. 13. a) Plot of the saturation IRM versus bulk magnetic susceptibility. The color of the symbols illustrates the magnitude of the foliation impressed by IRM. Fully white symbols correspond to a magnetic foliation lower than 1.003. b) Plot of M_{rs}/M_s ratio versus B_{cr}/B_c ratio for selected samples from different lithologies. The magnitude of the foliation $AMS_{\_IRM}$ is according to the color palette which is the same on both plots.

As expected from the rock lithology, samples from intrusive rocks have clearly MD grains. On the contrary, samples from volcanics with the largest $AMS_{\_IRM}$ foliation have large M_{rs}/M_s ratio and low B_{cr}/B_c values corresponding to fine (SD) magnetic grains. Samples from the metamorphic rocks with titanohematite have the highest M_{rs}/M_s ratio. However, their magnetic carrier is titano-hematite not magnetite. For some samples, especially those with high B_{cr} values, the maximum field of 1 Tesla used for the experiment is not a saturation field. A higher saturating field would probably slightly reduce the M_{rs}/M_s ratio (**Supplementary Figure S7**). While samples with high impressed foliation have high M_{rs}/M_s ratio, these samples have a wide range of B_{cr} or B_c values. FORC data (**Supplementary Figure S8**) on samples confirm that small grain size is the key factor for large $AMS_{\_IRM}$ with samples containing titanomagnetite or pyrrhotite.

The contribution of paramagnetic minerals to the magnetic susceptibility is negligible in volcanic and intrusive rocks. The high/low ratio of IRM/κ and the high/low degree of $AMS_{\_IRM}$ may therefore be suitable proxies of grain size from single domain grains in rapidly cooled volcanic rocks to multidomain magnetite grains in intrusive rocks.

6.2 Relation of $AMS_{\_IRM}$ with IRM during AF or thermal demagnetization

In samples from volcanic rocks, the $AMS_{\_IRM}$ foliation increases with IRM intensity (Fig. 14a), but during AF demagnetization, the impressed IRM foliation rapidly decreases and is

nearly removed by an AF tumbling at 20 mT while more than half of the magnetic foliation is acquired above 30mT during the IRM acquisition.

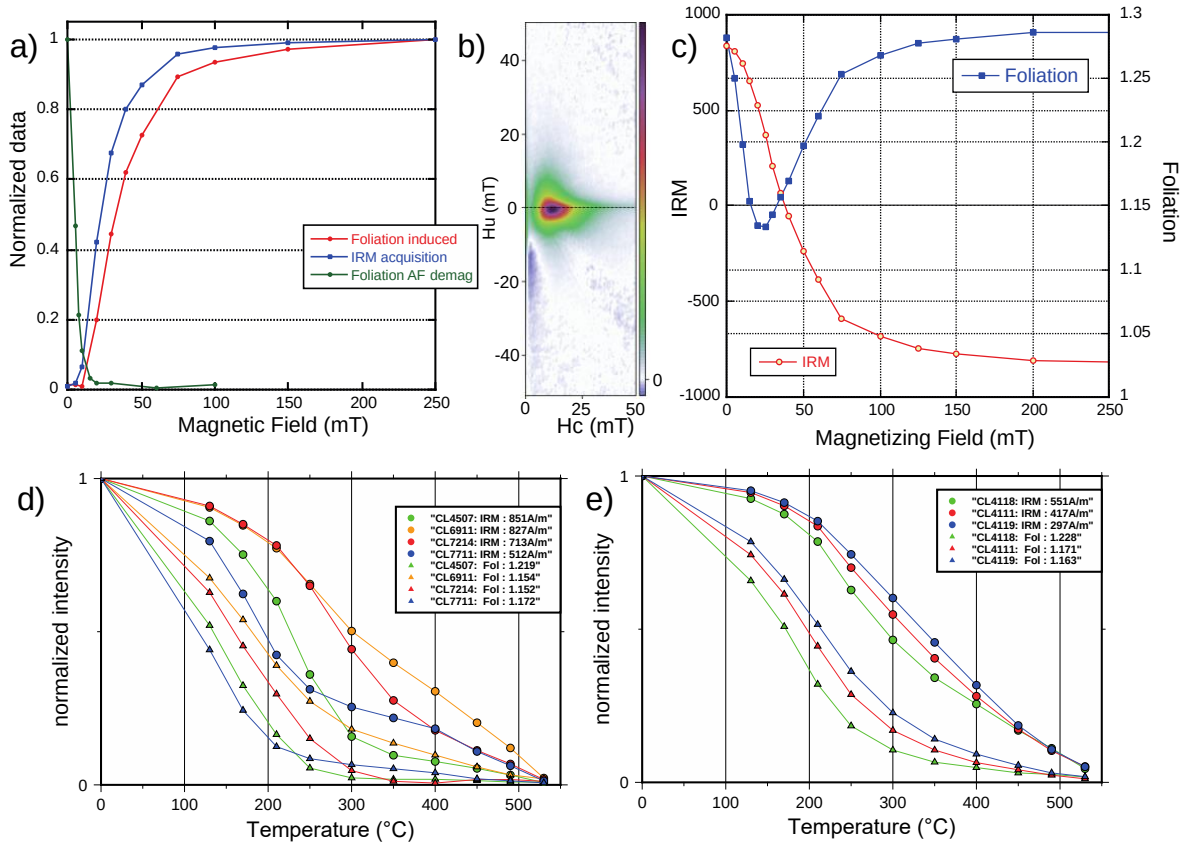

Fig. 14. a) Comparison of the changes in magnetic foliation during IRM acquisition and its subsequent AF demagnetization. (Sample CL1404a); b) FORC obtained for the sample as in (a)*;* c) Evolution of the $AMS_{\_IRM}$ and IRM during a reverse field IRM acquisition for one sample from Holocene rapidly cooled lava flow tops (CL7209). d, e) Decrease in $AMS_{\_IRM}$ foliation (triangles) upon progressive thermal demagnetization of the IRM (circles) for two sets of samples; (d) rapidly cooled lava flow tops and (e) samples from juvenile basaltic clast of a pyroclastic deposit (CL41). The IRM were normalized to the initial values (indicated on the plot) prior to the thermal demagnetization of the IRM. The AMS was measured at room temperature after each demagnetization step. The normalized data for the foliation is calculated using the following formula $(f_i\text{-}1)/(f_0\text{-}1)$ (f_0 is the foliation value at IRM saturation)

During reverse IRM acquisition, $AMS_{\_IRM}$ does not vanish at B_{cr} value but its minimum value is observed below B_{cr} (Fig. 14c).

For monitoring thermal stepwise demagnetization of saturation IRM and the associated $AMS_{\_IRM}$, both acquired at room temperature, we selected samples from rapidly cooled volcanics with SD titanomagnetites that record large $AMS_{\_IRM}$ foliation. This $AMS_{\_IRM}$ is progressively removed by thermal demagnetization but with unblocking temperatures systematically lower by 100 to 150°C than those of the IRM (Fig. 14d,e).

7.0 Discussion

7.1 Origin of the IRM impressed magnetic foliation

Hysteresis parameters of rapidly cooled volcanic rocks point to SD behavior in good agreement with the study of Lanci (2010) ($M_{rs}/M_s > 0.4$ and $B_{cr}/B_c \sim 1$). The nearly isotropic fabric of the rocks prior to IRM acquisition permits to discard a preferential distribution of elongated uniaxial SD grains. M_{rs}/M_s ratio above 0.5 could be explained by SD grains of titanomagnetites with multiaxial anisotropy (Dunlop and Özdemir, 1997). In that case, the magnetic susceptibility will be reduced in the direction of the IRM as suggested by Lanci (2010). Microscope observations indicate small (a few µm) titanomagnetite grains with a dendritic structure in rapidly-cooled flow tops. As discussed by (Shaar and Feinberg, 2013), the size of the dendrites exceeds the SD-MD threshold for crystals with simple geometry. Yet these samples exhibit SD behavior in hysteresis data (Fig. 13b) and FORC (**Supplementary Figure S8**). Shaar and Feinberg (2013) also indicated that dendrites have significant anisotropy but they point out that the question remains open as to why a sample that contains a very large number of dendrites is anisotropic. Impressed $AMS_{\_IRM}$ in such samples needs further investigations. Lanci (2010) found that this impressed fabric is easily removed by AF supporting that it is carried by a low coercivity phase. We observe, however, that AF demagnetization at low fields (< ~50 mT) is especially efficient to reduce the $AMS_{\_IRM}$ fabric acquired at higher fields (~> 50 mT). A low coercivity carrier cannot explain this very strong asymmetry between the AMS acquisition by IRM and its subsequent rapid destruction by AF (Fig. 14a). An asymmetry between two opposite IRMs in fields lower than the saturating field is, however, observed at low fields in the test for multiaxial anisotropy proposed by (Mitra et al., 2011) (**Supplementary Figure S9.**).

The faster thermal decrease of the $AMS_{\_IRM}$ foliation compared to IRM (Fig. 14d,e) suggests a larger contribution of Ti-rich titanomagnetite or a larger contribution of the smallest grains to the $AMS_{\_IRM}$. The fact that AF demagnetization rapidly removes the impressed fabric is intriguing. During progressive reverse IRM acquisition, the magnetic foliation increases until saturation. The strong IRM acquired above B_{cr} value exerts somehow a significant control on the impressed foliation but this is not observed with AF demagnetization.

Large $AMS_{\_IRM}$ is also observed in metamorphic volcaniclastic rocks with large (a few tens of µm) titanohematite grains. No ilmenite lamellas but rutile inclusions are observed. Further work, especially TEM imaging, is needed to check the internal structure of the titanohematite (McEnroe et al., 2009).

A maximum foliation of 1.8 was found for the $AMS_{\_IRM}$ in one of these metamorphic volcanoclastic sample (**Supplementary Figure S10**). Its $AMS_{\_IRM}$ decreases more rapidly than the IRM during the AF demagnetization of this IRM but this decrease is less marked than in volcanic rocks (Fig. 14a).

The large impressed AMS is found in rocks with magnetic carriers (titanomagnetite, pyrrhotite) showing a strong out-of-phase magnetic susceptibility (Hrouda et al., 2022, 2020). The out-of-phase signal of the AMS was checked for one sample without IRM applied and three samples with an $AMS_{\_IRM}$. The out-of-phase magnetic susceptibility is only 1 to 6 % of

the in-phase susceptibility. A slight out-of-phase AMS (foliation of 1.02) is found in the sample with an almost isotropic in-phase AMS prior to IRM acquisition. The out-of-phase $AMS_{\_IRM}$ is nearly four times higher than the in-phase $AMS_{\_IRM}$ (**Supplementary Figure S11**) with one sample having a foliation up to 2.17 while the in-phase foliation was of 1.27. This observation highlights the contribution of titanomagnetite to the $AMS_{\_IRM}$.

We did not check on a sufficient large number of samples the relation between the AC field value and the $AMS_{\_IRM}$ anisotropy. In sample CL6915A from a lava flow (Table S1), the degree of foliation increases by only 20% from 1.136 to 1.164 with AC fields of 50 to 700 Am^{-1} respectively.

7.2 Origin of the static AF impressed magnetic lineation

As discussed in previous papers, the AF-impressed lineation is usually interpreted as the result of domain alignment in MD particles. However, the AF-impressed lineation is better observed in samples from volcanic rocks with PSD-like hysteresis parameters than in intrusive rocks with large MD particles of magnetite. This suggests that the largest grains, the shape preferred orientation (SPO) of which contribute to the AMS in plutonic rocks, are not involved in AF-impressed anisotropy

In lavas with an AF-induced AMS lineation, the hysteresis parameters point to mean magnetic grain sizes in the PSD range. However, microscope observations show that 5 to 10 µm titanomagnetite grains are present and correspond to MD grain size. In some volcanic rocks, susceptibility is field-dependent and was interpreted as evidence for wall displacements in multidomain titanomagnetite (Jackson et al. 1998). Indeed, in these samples, the AF-impressed magnetic lineation increases with AC field (1.006 to 1.03). The magnetic lineation is, however, also observed in samples without any susceptibility field-dependence. In our collection of Holocene lavas, a few flows present a significant initial anisotropy compared to the one impressed by static AF. These samples also exhibit a large field-dependent susceptibility ($\kappa_{700\ A/m}/\kappa_{50\ A/m} > 1.5$) and enhancement (1.057 to 1.086) in the degree of anisotropy similar to the one reported in other studies (De Wall, 2000). At this stage, our results indicate that the AF impressed lineation is not systematically related to a specific type of titanomagnetite showing susceptibility field-dependence.

Our observations from a large collection of samples indicate that the magnetic lineation is mainly carried by small MD grains (~5µm) without significant SPO anisotropy. The anisotropy impressed by static AF is thus mainly added to the previous natural fabric.

8.0 Conclusions

Our results permit to highlight several points about the effect of high fields on the AMS and are summarized below:

1) AF and IRM acquisition induce significant changes in bulk susceptibility as already discussed in previous papers (Biedermann et al., 2017; Jordanova et al., 2007). Volcanic rocks with titanomagnetite are especially prone to these changes. The magnetic susceptibility of these samples also shows a strong dependence on the AC field value used for the measurement, consistent with previous work on titanomagnetites (Jackson et al., 1998).

2) After application of an AF or an IRM, the change in the magnetic susceptibility is not a "reversible" process. In contrast changes in the magnetic fabric impressed by static AF or IRM is reversible (i.e. the same fabric can be removed by tumbling AF or thermal demagnetization, and impressed again or replaced by a new one along an other axis).
3) Static AF demagnetization may create a magnetic lineation parallel to the direction of the AF field or a magnetic foliation orthogonal to the AF field.
4) An IRM may create a large AMS foliation with Kmin along the IRM direction.
5) The grain size of the magnetic minerals appears to be the main parameter controlling a large IRM impressed foliation observed in various types of rocks (smallest grains/largest foliation).
6) The impressed fabrics are better observed in samples with titanomagnetites and titanohematite rather than in pure magnetite and hematite.
7) A correlation is clearly observed between the fabrics impressed by AF and by IRM. The magnetic foliation orthogonal to the AF field is observed in samples with a large IRM impressed foliation. The magnetic lineation acquired by static AF is better defined in samples without or with low IRM impressed anisotropy. The magnitude of the AF impressed lineation is dependent on the field applied during the AMS measurement for samples that also show a field-dependence of the susceptibility.
8) These impressed fabrics are reset by the subsequent application of AF or IRM. In nearly all cases, the subtraction of the natural AMS fabric to the fabric measured after AF or IRM acquisition, significantly improves the determination of the impressed fabric and of its prolate or oblate shape. The impressed fabric is thus mainly superimposed to the original fabric in particular when the original AMS is carried by paramagnetic minerals and oxides without an AF or IRM impressed fabric. In intrusive rocks, AF or IRM do not significantly modify the AMS carried by the shape preferred orientation (SPO) of magnetite.

In summary, the AF-impressed magnetic lineation is usually lower than 1.02 and, in samples with titanomagnetite carriers, it is enhanced by the AC field intensity applied during the AMS measurement. Using lower fields in susceptibility meters (<50 Am^{-1}) reduces the magnitude of the AF impressed anisotropy but with larger errors in the determination of the ellipsoid. The AF-impressed AMS is significant in volcanic samples without or with very low initial anisotropy ($P < 1.02$). Samples with a magnetic foliation orthogonal to the static AF field direction during demagnetization, also acquire a much larger foliation impressed by an IRM.

The AMS_{IRM} provides interesting information on the nature of the magnetic carriers and their possible multiaxial anisotropy. Using this artificial AMS as a proxy for the existence of multiaxial magnetic carriers seems to be an alternative to the method proposed by Mitra et al., (2011) and further discussed by Fabian (2012). Although the multiaxial anisotropy in SD grains seems to be an ad-hoc interpretation, further work is needed to better understand potential physical mechanisms leading to this strong impressed foliation, like the mineral magnetic composition (titanomagnetite, titanohematite and pyrrhotite) or the shape and texture of the particles, such as dendrites.

AF impressed fabrics have usually been attributed to MD grains. However, we find that, in samples from intrusive rocks with large MD grains, the well-defined initial AMS fabric due to the strong SPO of the magnetic carriers is not really affected by AF demagnetization.

It is always preferable to measure the AMS before performing static AF demagnetization. If this is not possible, the use of a tumbler during AF is the best option. Furthermore, as pointed out by Rochette et al. (1992), if the AMS directions are scattered in the natural state, this scattering may be due to the interaction of the AMS with the NRM. For example, in volcanic rocks, samples from lightning struck sites may have a large NRM and the IRM impressed anisotropy described here may be the cause of the AMS scatter. In this case, tumbling AF demagnetization may help to restore the intrinsic magnetic structure.

ACKNOWLEDGMENTS

We thank Melina Macouin (Géosciences Toulouse) for the measurement of the out-of-phase signal of 4 samples with the KLY5 and François Demory (CEREGE) for his help with the MFK1 and LDA5 instruments. Some of the figures were done with the GMT software. The acquisition of the VSM8600 and MFK2-FA by the Laboratoire des Sciences du Climat et de l'Environnement (LSCE) was financially supported by the Paris Ile-de-France Region – DIM “Matériaux anciens et patrimoniaux”, the Institut National des Sciences de l'Univers (INSU) and the LSCE. We thank Francis Gouttefangeas from the ScanMAT/CMEBA platform for his help with the SEM/EDS data. Francisco Gutierrez provided the samples from the Miocene intrusive rocks from Central Chile.

REFERENCES

Aminov, J., Roperch, P., Dupont-Nivet, G., Cordier, C., Guillot, S., Glodny, J., Timmerman, M.J., Wilke, M., Lagroix, F., Ding, L., Mamadjanov, Y., submitted. Miocene metamorphism and deformation of the Central Pamir constrained by geochronological and paleomagnetic data from volcaniclastic rocks in the Bartang area, Tajikistan. Tectonophysics.

Bhathal, R.S., Stacey, F.D., 1969. Field-induced anisotropy of magnetic susceptibility in rocks. Pure Appl. Geophys. 76, 123–129. https://doi.org/10.1007/BF00877845

Biedermann, A.R., Jackson, M., Bilardello, D., Feinberg, J.M., Brown, M.C., McEnroe, S.A., 2017. Influence of static alternating field demagnetization on anisotropy of magnetic susceptibility: Experiments and implications. Geochem. Geophys. Geosyst. 18, 3292–3308. https://doi.org/10.1002/2017GC007073

Bilardello, D., Biedermann, A.R., 2022. Practical Magnetism VIII: reporting and visualization of magnetic anisotropy data. The IRM Quartely 32, 18.

Borradaile, G.J., Henry, B., 1997. Tectonic applications of magnetic susceptibility and its anisotropy. Earth Sci. Rev. 42, 49–93. https://doi.org/10.1016/S0012-8252(96)00044-X

De Wall, H., 2000. The Field-Dependence of AC Susceptibility in Titanomagnetites: Implications for the Anisotropy of Magnetic Susceptibility. Geophys. Res. Lett. 27, 2409–2411. https://doi.org/10.1029/2000GL008515

Dunlop, D.J., Özdemir, Ö., 1997. Rock magnetism: fundamentals and frontiers. Cambridge university press.

Fabian, K., 2012. Comment on ‘Detecting uniaxial single domain grains with a modified IRM technique’ by R. Mitra, L. Tauxe and J. S. Gee. Geophys. J. Int. 191, 42–45. https://doi.org/10.1111/j.1365-246X.2012.05478.x

Henry, B., Jordanova, D., Jordanova, N., Hus, J., Bascou, J., Funaki, M., Dimov, D., 2007. Alternating field-impressed AMS in rocks. Geophys. J. Int. 168, 533–540. https://doi.org/10.1111/j.1365-246X.2006.03235.x

Hrouda, F., 1982. Magnetic anisotropy of rocks and its application in geology and geophysics. Geophysical Surveys 5, 37–82. https://doi.org/10.1007/BF01450244

Hrouda, F., Chadima, M., Ježek, J., 2022. Anisotropy of Out-of-Phase Magnetic Susceptibility and Its Potential for Rock Fabric Studies: A Review. Geosciences 12, 234. https://doi.org/10.3390/geosciences12060234

Hrouda, F., Ježek, J., Chadima, M., 2020. Anisotropy of out-of-phase magnetic susceptibility as a potential tool for distinguishing geologically and physically controlled inverse magnetic fabrics in volcanic dykes. Physics of the Earth and Planetary Interiors 307, 106551. https://doi.org/10.1016/j.pepi.2020.106551

Jackson, M., Moskowitz, B., Rosenbaum, J., Kissel, C., 1998. Field-dependence of AC susceptibility in titanomagnetites. Earth Planet. Sci. Lett 157, 129–139. https://doi.org/10.1016/S0012-821X(98)00032-6

Jelinek, V., 1981. Characterization of the magnetic fabric of rocks. Tectonophysics 79, T63–T67. https://doi.org/10.1016/0040-1951(81)90110-4

Jordanova, D., Jordanova, N., Henry, B., Hus, J., Bascou, J., Funaki, M., Dimov, D., 2007. Changes in mean magnetic susceptibility and its anisotropy of rock samples as a result of alternating field demagnetization. Earth Planet. Sci. Lett 255, 390–401. https://doi.org/10.1016/j.epsl.2006.12.025

Lanci, L., 2010. Detection of multi-axial magnetite by remanence effect on anisotropy of magnetic susceptibility. Geophys. J. Int. 181, 1362–1366.

Li, L., Dupont-Nivet, G., Najman, Y., Kaya, M., Meijer, N., Poujol, M., Aminov, J., 2022. Middle to late Miocene growth of the North Pamir. Basin Research 34, 533–554. https://doi.org/10.1111/bre.12629

Liu, Q.S., Yu, Y.J., Deng, C.L., Pan, Y.X., Zhu, R.X., 2005. Enhancing weak magnetic fabrics using field-impressed anisotropy: application to the Chinese loess. Geophys. J. Int. 162, 381–389.

McEnroe, S.A., Brown, L.L., Robinson, P., 2009. Remanent and induced magnetic anomalies over a layered intrusion: Effects from crystal fractionation and magma recharge. Tectonophysics 478, 119–134.

Mitra, R., Tauxe, L., Gee, J.S., 2011. Detecting uniaxial single domain grains with a modified IRM technique: Detecting uniaxial single domain grains. Geophys. J. Int. 187, 1250–1258. https://doi.org/10.1111/j.1365-246X.2011.05224.x

Poblete, F., Roperch, P., Arriagada, C., Ruffet, G., Ramírez de Arellano, C., Hervé, F., Poujol, M., 2016. Late Cretaceous–early Eocene counterclockwise rotation of the Fueguian Andes and evolution of the Patagonia–Antarctic Peninsula system. Tectonophysics 668–669, 15–34. https://doi.org/10.1016/j.tecto.2015.11.025

Potter, D.K., Stephenson, A., 1990a. Field-impressed magnetic anisotropy in rocks. Geophys. Res. Lett. 17, 2437–2440. https://doi.org/10.1029/GL017i013p02437

Potter, D.K., Stephenson, A., 1990b. Field-impressed anisotropies of magnetic susceptibility and remanence in minerals. J. Geophys. Res. Solid Earth 95, 15573–15588.

https://doi.org/10.1029/JB095iB10p15573

Rochette, P., Jackson, M., Aubourg, C., 1992. Rock magnetism and the interpretation of anisotropy of magnetic susceptibility. Rev. Geophys. 30, 209–226. https://doi.org/10.1029/92RG00733

Roperch, P., Chauvin, A., Lara, L.E., Moreno, H., 2015. Secular variation of the Earth's magnetic field and application to paleomagnetic dating of historical lava flows in Chile. Phys. Earth Planet. Inter. 242, 65–78. https://doi.org/10.1016/j.pepi.2015.03.005

Roperch, P., Chauvin, A., Le Pennec, J.-L., Lara, L.E., 2014. Paleomagnetic study of juvenile basaltic-andesite clasts from Andean pyroclastic density current deposits. Phys. Earth Planet. Inter. 227, 20–29. https://doi.org/10.1016/j.pepi.2013.11.008

Schöbel, S., Wall, H. de, Rolf, C., 2013. AMS in basalts: is there a need for prior demagnetization? Geophys. J. Int. 195, 1509–1518. https://doi.org/10.1093/gji/ggt325

Shaar, R., Feinberg, J.M., 2013. Rock magnetic properties of dendrites: insights from MFM imaging and implications for paleomagnetic studies. Geochem. Geophys. Geosyst. 14, 407–421. https://doi.org/10.1002/ggge.20053

Violat, C., Daly, L., 1971. Anisotropie provoquée sur des roches volcaniques par action d'un champ alternatif. Compt. Rend. Acad. Sci. Paris B 273, 158–161.

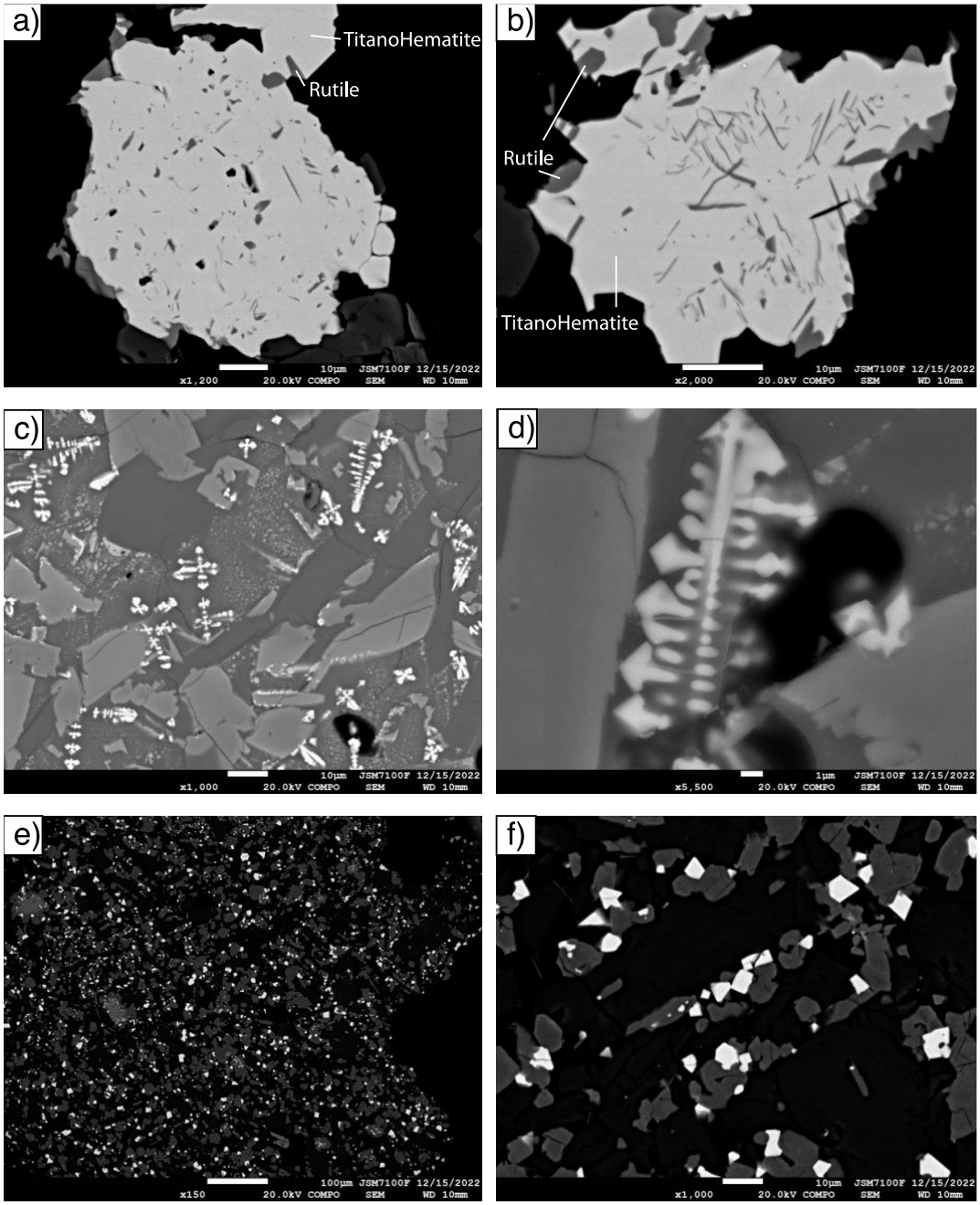

Supplementary Figure S1. SEM images of Ti, Fe oxides in metamorphic sediments from Pamir (a, b) with large titanohematite grains with rutile inclusions; c,d) rapidly cooled Holocene volcanics with titanomagnetite dentrites (Southern Chile) and e,f) titanomagnetite grains in massive Holocene lava flows (Southern Chile).

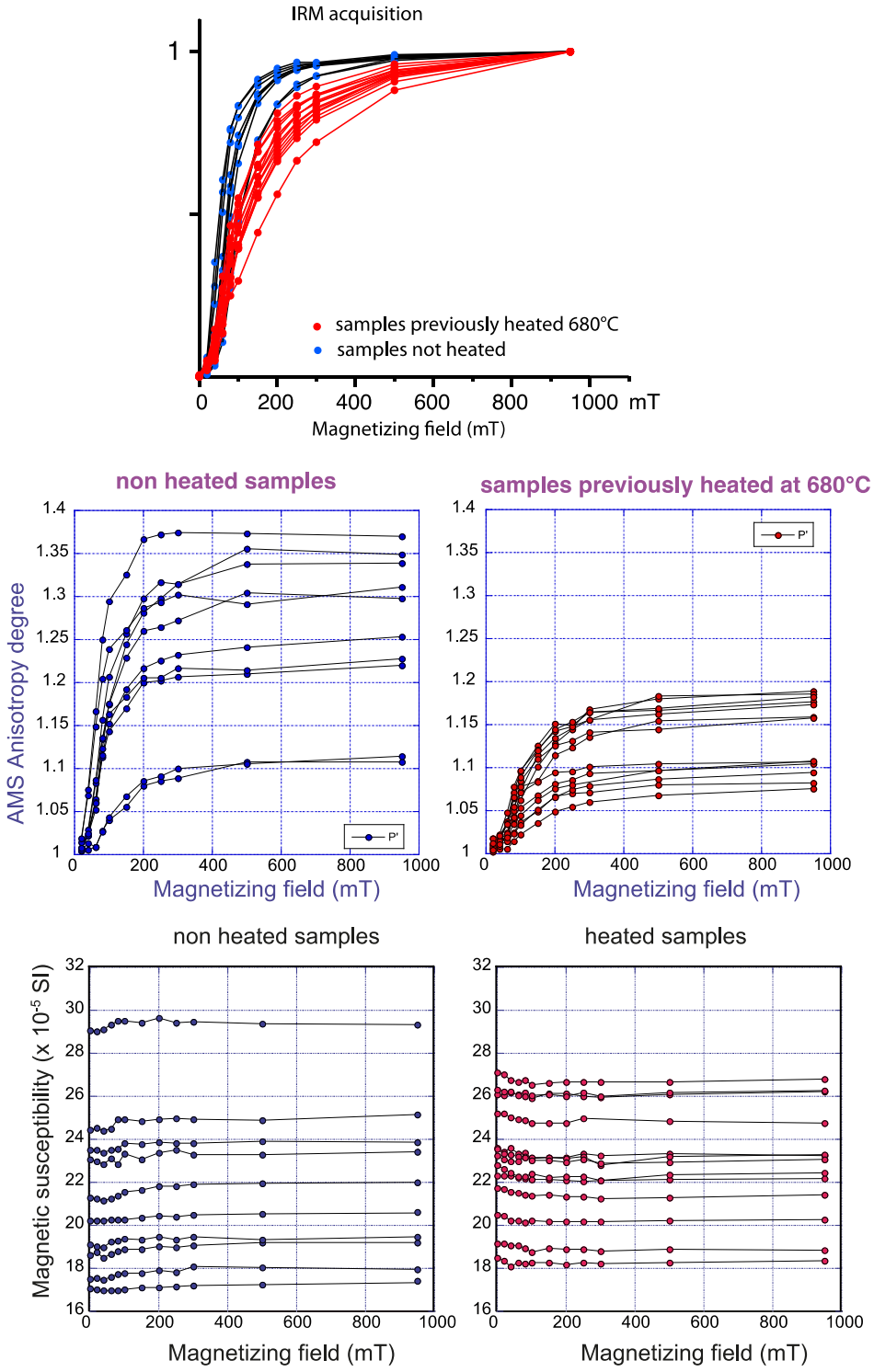

Supplementary Figure S2. Top) normalized plot of IRM acquisition in metamorphic volcanoclastic sediments with titanohematite (Aminov et al., submitted). Middle) Anisotropy degree of the difference ellipsoids at each step of the IRM acquisition. Bottom) Mean magnetic susceptibility at each step of the IRM acquisition.

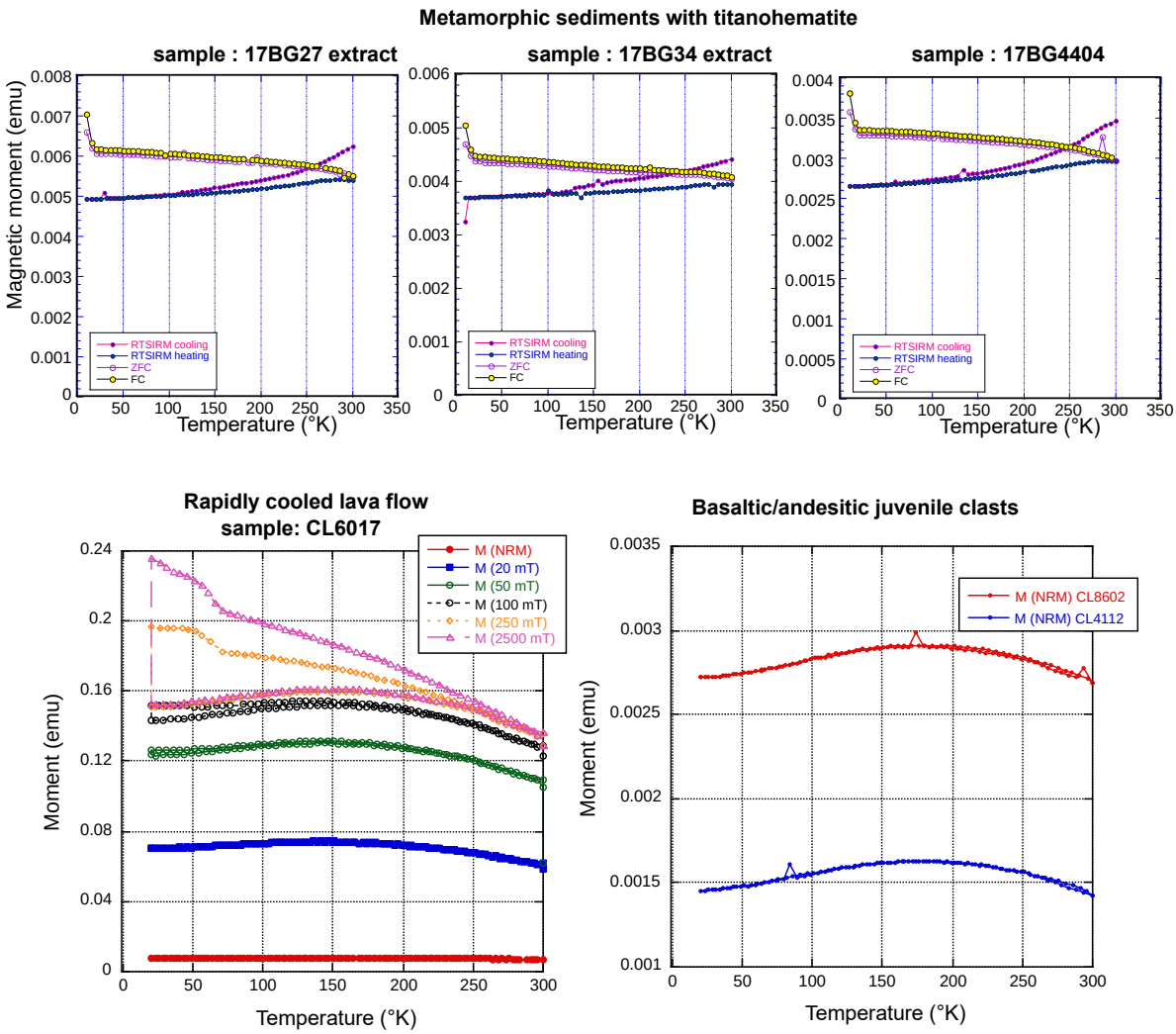

Supplementary Figure S3. Top) examples of magnetization measurements at low temperature for three samples of sediments with titanohematite from the Pamir. (RTSIRM: room temperature saturation IRM cooling and heating cycle followed by Zero Field Cooled (ZFC) and Field Cooled measurements (FC). Extract indicates that the samples were enriched in magnetic minerals using a magnet. Bottom left) NRM and IRM were measured at low temperatures. For each cycle, the IRM was given first at room temperature and at 20°K. Bottom right) NRM measurements at low temperatures for two different samples.

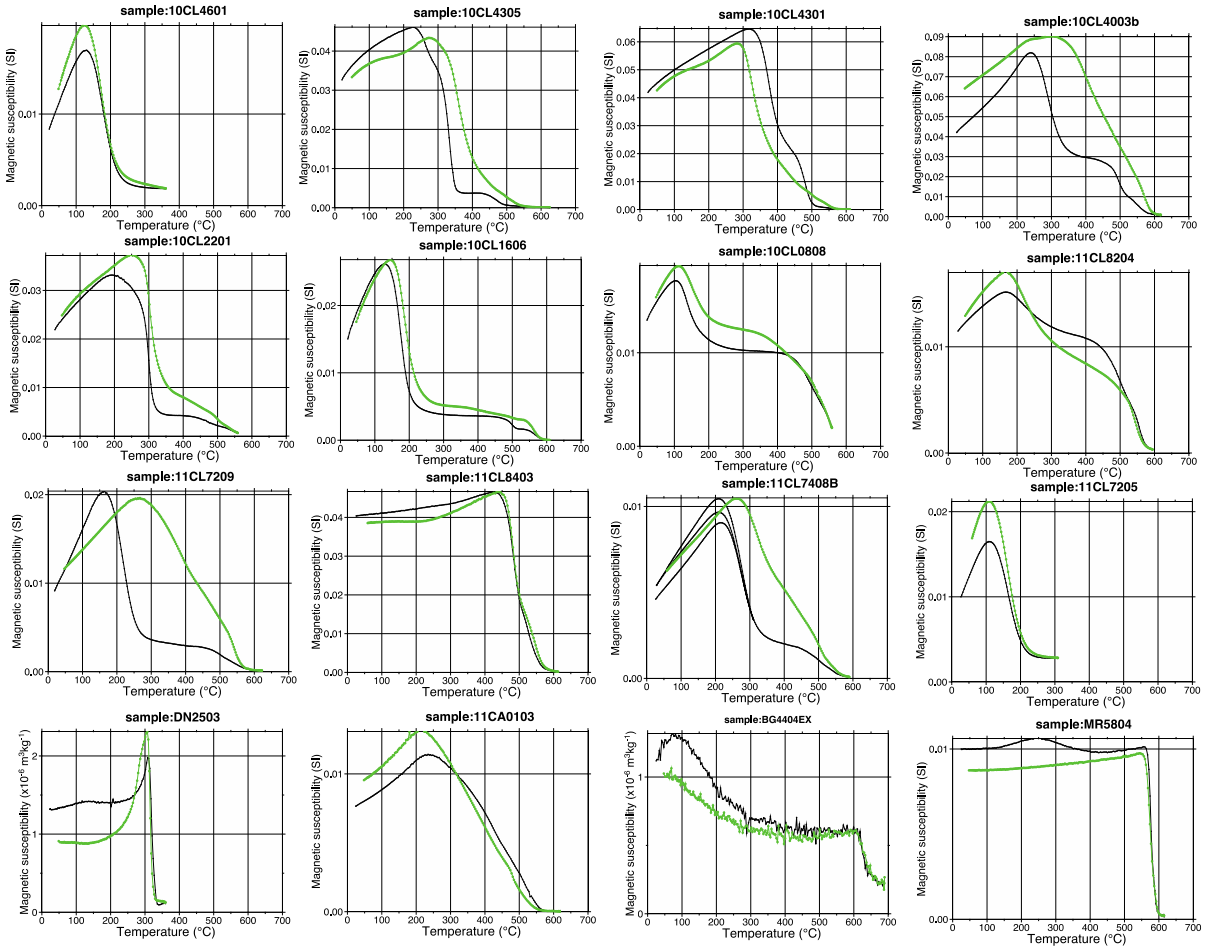

Supplementary Figure S4. Magnetic susceptibility versus temperature for samples of volcanic rocks, except, metamorphic sediments with pyrrhotite (DN2506), bricks (11CA0103), metamorphic sediments with titanohematite (BG4404EX) and intrusive rocks (MR5804)

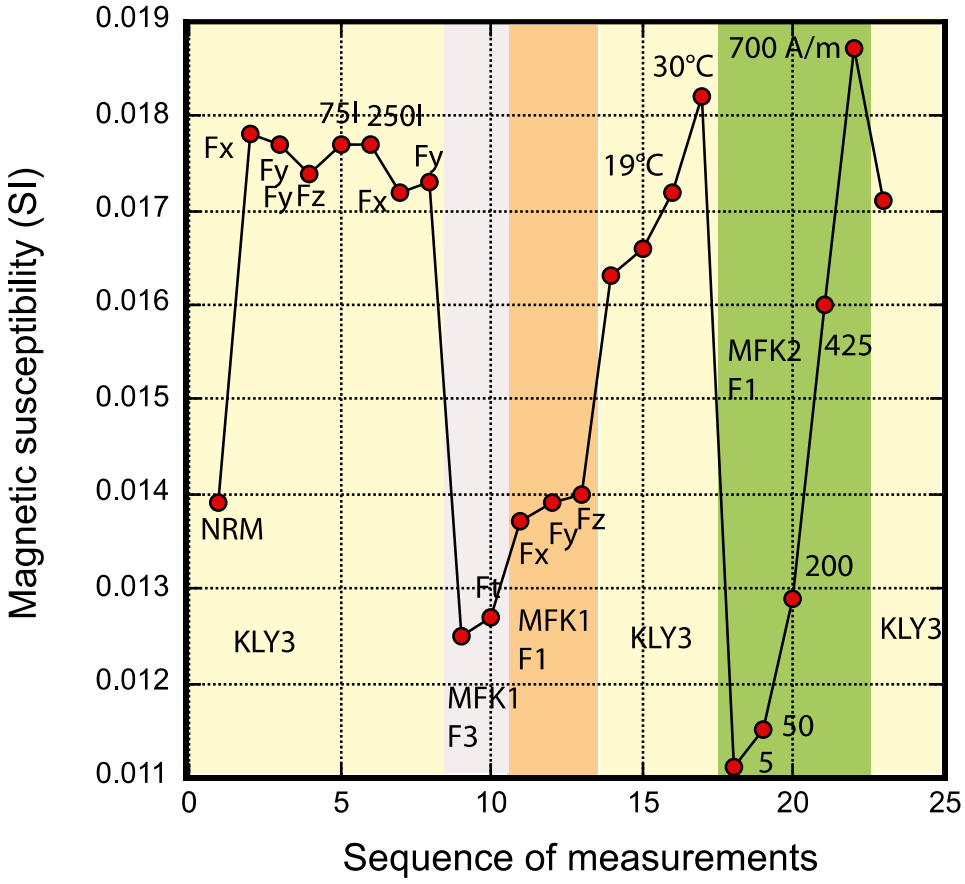

Supplementary Figure S5. Magnetic susceptibility measurement after NRM, AF demagnetization at 70mT upon X (Fx), Y (Fy), Z, (Fz), a tumbler at 100 mT (Ft); IRM acquisition at 75mT (75I), 250 mT (250 mT) with different instrument (KLY3 standard), MFK1 at 200 A/m with high frequency (F3) or low Frequency (F1) and the MFK2 at low frequency (F1) and different field value (5, 50, 200, 425 and 700 A/m). Most measurement were done at room temperature (~20°C) except for one measurement for which the sample was slightly heated at ~30°C.

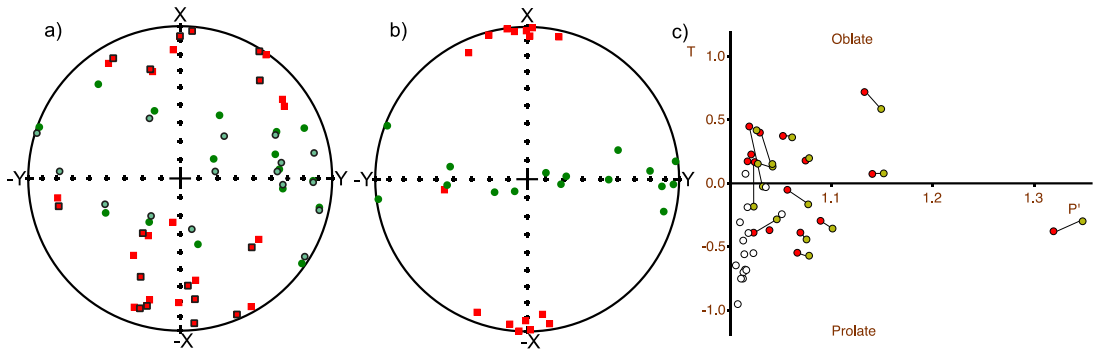

Supplementary Figure 6. AMS data in intrusive rocks before and after AF demagnetization at 70mT along X. a) stereonet of the direction of the maximum (squares) and minimum axes before and after AF demagnetization. b) stereonet of the difference ellipsoids. C) T-P' plot of the AMS parameter before (red circles), after AF (green circles) and difference tensors (white circles).

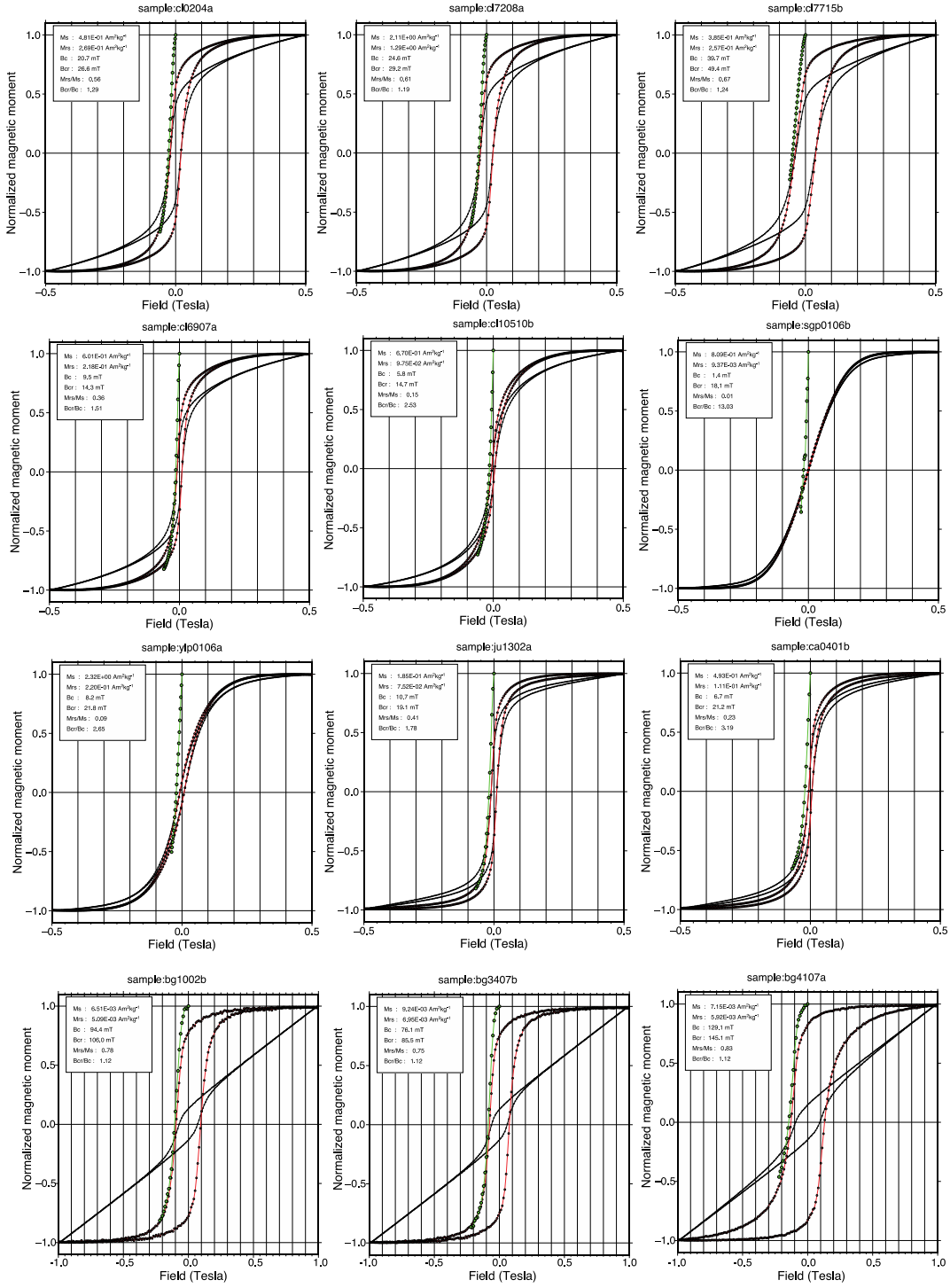

Supplementary Figure S7. Examples of hysteresis data obtained with a VSM. Samples from volcanic rocks (cl0204a, cl7208a, cl7715b, cl6907a, cl10510b), intrusive rocks (sgp0106b, ylp0106a), bricks (ju1302a, ca0401b) and metamorphic volcanoclastics (Pamir samples bg1002b, bg3407b, bg4107a).

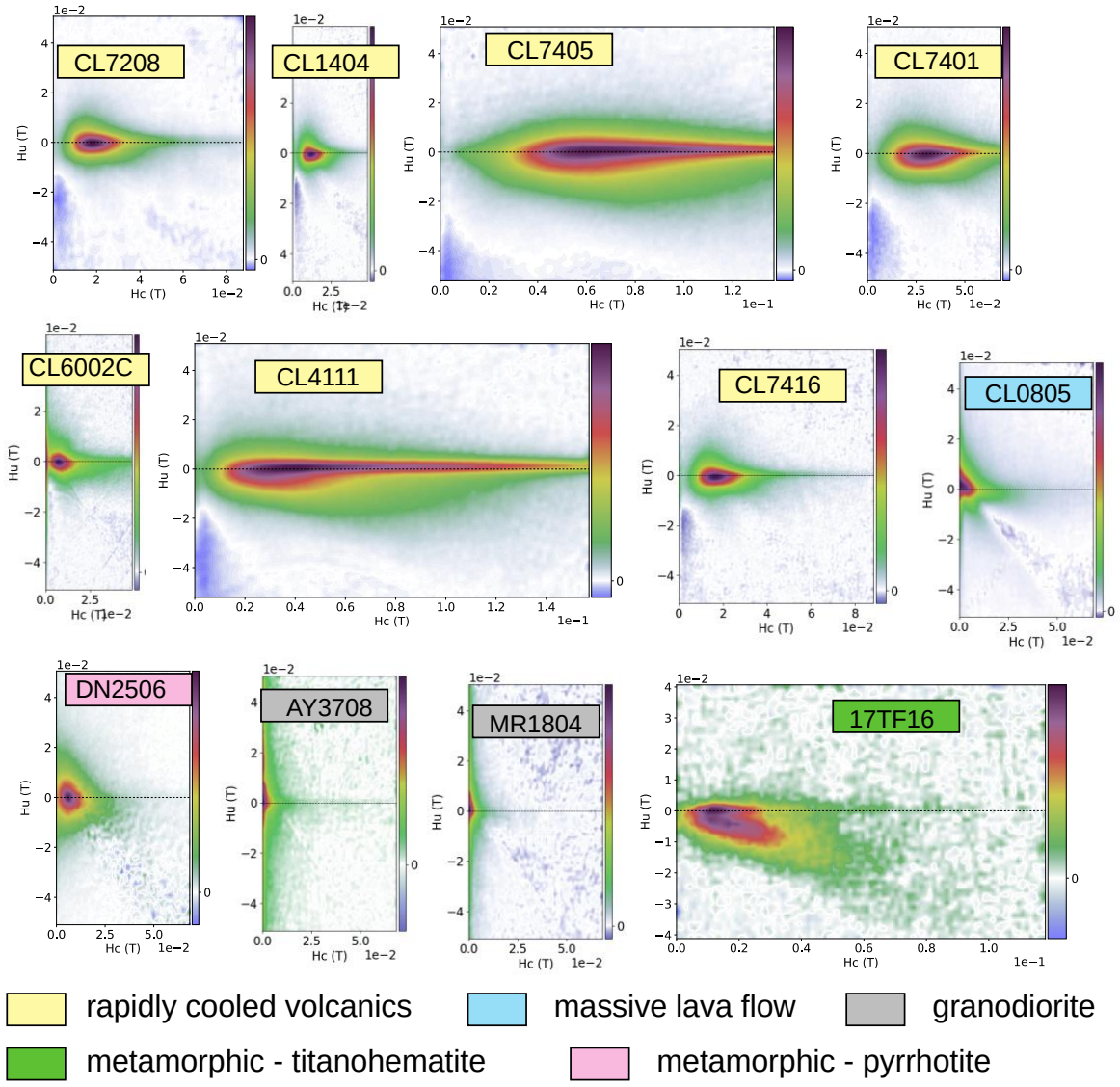

Supplementary Figure S8. Examples of FORC diagrams in various types of samples.

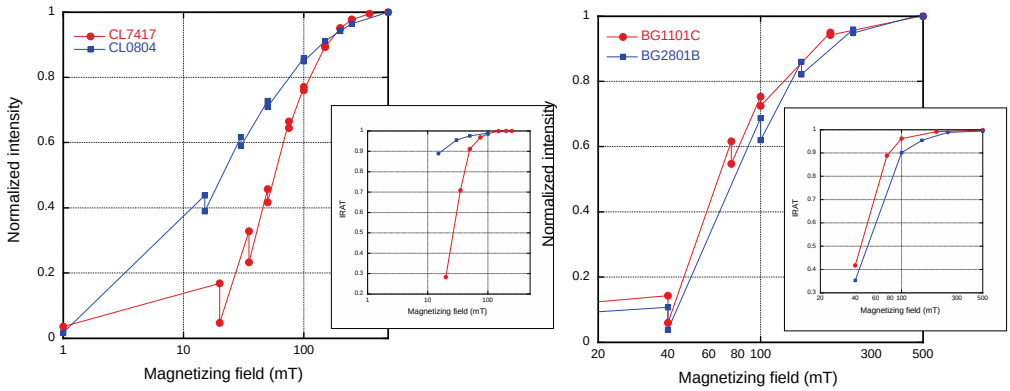

Supplementary Figure S9. Acquisition of IRM in samples from volcanic rocks (left) and in metamorphic volcanoclastic rocks (right).At each step, the IRM acquisition was done in two opposite directions following the procedure given in Mitra et al. (2011). IRAT is the ratio of the two opposite IRMs at each step of IRM acquisition.

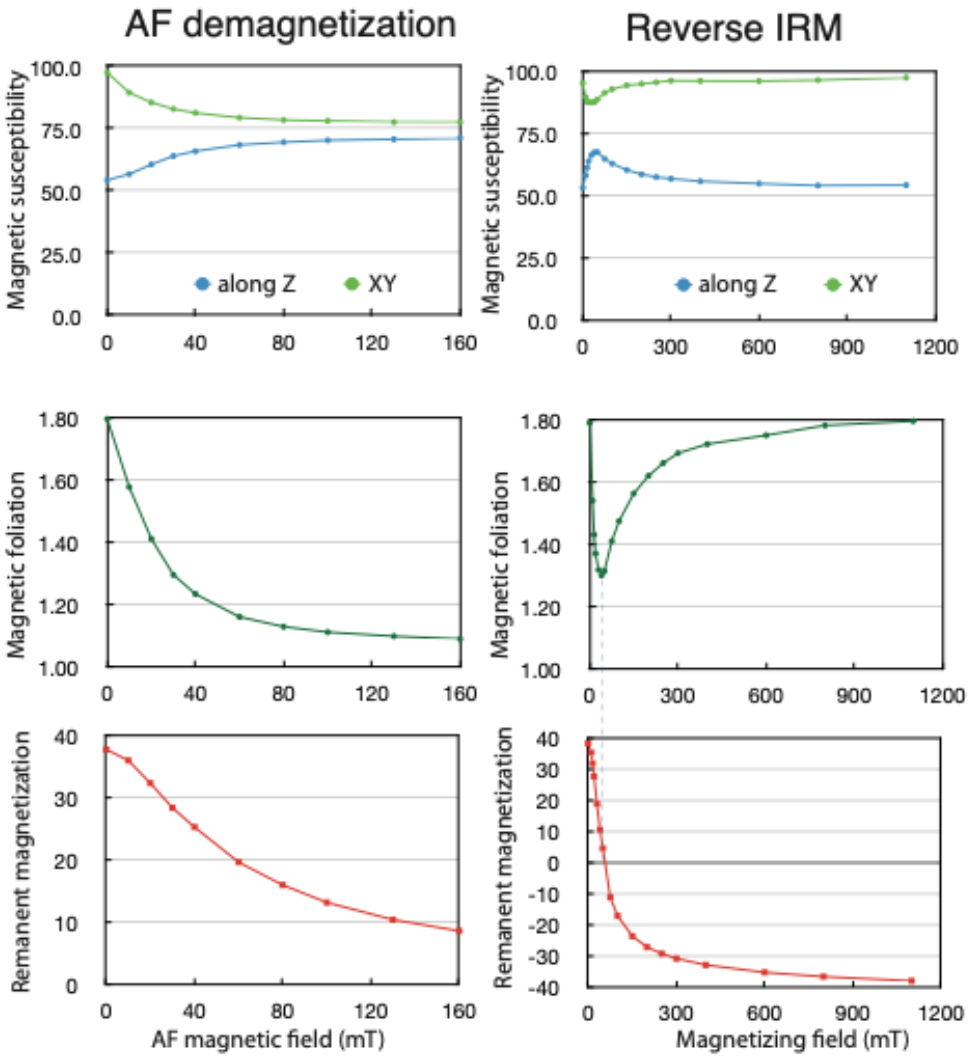

Supplementary Figure S10. Variation of the magnetic susceptibility during the AF demagnetization of an IRM (left) and the acquisition of a reverse IRM. The magnetic susceptibility was measured along the Z axis (direction of the IRM) and in the orthogonal XY plane. The AF demagnetization using the 2G static AF degausser was done only along Z.

The sample is a consolidated powder of metamorphic rock with titanohematite.

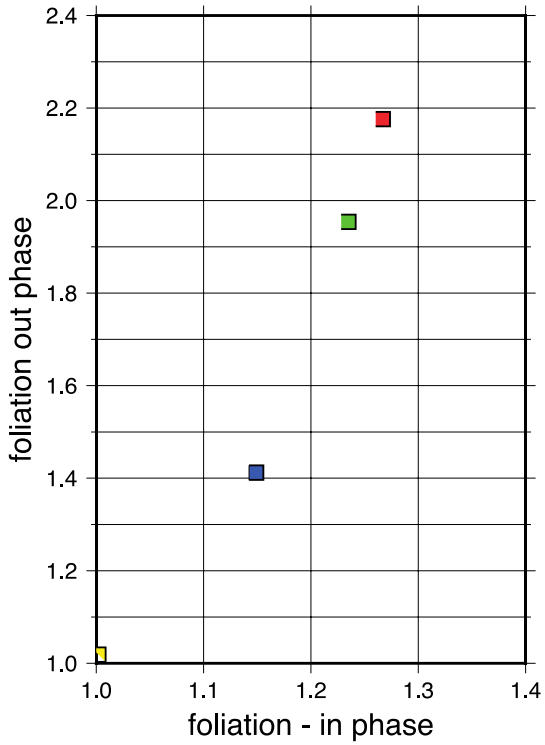

Supplementary Figure S11. Comparison of the foliation value in in phase and out of phase measurements with the KLY5 susceptibilitymeter for 4 samples from rapidly cooled lavas. The sample without foliation is without IRM while the three others were given an SIRM.